



TECHNISCHE
UNIVERSITÄT
WIEN
Vienna | Austria

Diplomarbeit

Influence of human mass and posture on the rollover characteristics of carriages

ausgeführt zum Zwecke der Erlangung des akademischen Grades eines
Diplom-Ingenieurs unter der Leitung von

Univ.Prof. Dipl.-Ing. Dr.techn. Heinz-Bodo Schmiedmayer
E325

Institut für Mechanik und Mechatronik
und

Dr.phil. Josef Kastner

eingereicht an der Technischen Universität Wien

Fakultät für Maschinenwesen und Betriebswissenschaften

von

Christof Binder
Matr.Nr.: 0826115
Mayerhofgasse 7/13
1040 Wien

Wien, am 6. April 2016

Christof Binder

Eidesstattliche Erklärung

Ich habe zur Kenntnis genommen, dass ich zur Drucklegung meiner Arbeit unter der Bezeichnung

DIPLOMARBEIT

nur mit Bewilligung der Prüfungskommission berechtigt bin.

Ich erkläre weiters Eides statt, dass ich meine Diplomarbeit nach den anerkannten Grundsätzen für wissenschaftliche Abhandlungen selbstständig ausgeführt habe und alle verwendeten Hilfsmittel, insbesondere die zugrunde gelegt Literatur genannt habe.

Weiters erkläre ich, dass ich dieses Diplomarbeitsthema bisher weder im In- noch im Ausland (einer Beurteilerin/einem Beurteiler zur Begutachtung) in irgendeiner Form als Prüfungsarbeit vorgelegt habe und dass diese Arbeit mit der vom Begutachter beurteilten Arbeit übereinstimmt.

Wien, am 6. April 2016

Christof Binder

Danksagung

An dieser Stelle möchte ich mich bei Ao.Univ.Prof. Dipl.-Ing. Dr.techn. Heinz-Bodo Schmiedmayer und Dr.phil. Josef Kastner für die kompetente Betreuung und Hilfestellung im Zuge dieser Diplomarbeit bedanken.

Großer Dank gebührt auch meiner Familie, insbesondere meinen Eltern Irmagard und Robert Binder, da sie mich im Laufe meines Studiums stets unterstützte.

Ein besonderes Dankeschön richte ich an meine Freunde Ivo Steinbrecher und Bernhard Hopfner, die mir immer für rege Diskussionen, Rat und Tat zur Verfügung standen.

Kurzfassung

Diese Diplomarbeit handelt vom Einfluss der menschlichen Masse und Haltung auf das Kippverhalten im Gespannfahren. Dies ist insbesondere für den Wettkampf von Interesse. Um die optimale Fahrer- und Beifahrerhaltung zu finden, werden Simulationen für stationäre Kurvenfahrt auf der Ebene ohne Schräglage durchgeführt.

Ein Weg um vereinfachte Modelle der Kutschen bezüglich ihrer Trägheitstensoren zu erstellen, sowie die Ergebnisse für eine Marathon- und eine Dressurkutsche werden vorgestellt.

Weiters werden charakteristische Körperhaltungen von Fahrer und Beifahrer identifiziert und mittels des Hanavan-Modells [6] mathematisch modelliert. Diese identifizierten Haltungen werden des weiteren bezüglich der Empfindlichkeit des Trägheitstensors und der Schwerpunktslage bezüglich kleiner Abweichungen der Haltung analysiert.

Abschließend wird das erstellte dynamische Modell von Kutsche inklusive Fahrer und Beifahrer vorgestellt und für Simulationen angewandt, sowie die Ergebnisse für unterschiedliche Kombinationen von Fahrer und Beifahrerhaltung präsentiert. Auch einige Sonderfälle des dynamischen Verhaltens bei Kurvenfahrt, wie enge Kurven oder der Einfluss von Beschleunigung, werden untersucht.

Abstract

This diploma thesis investigates the influence of human mass and posture on the rollover characteristics of carriages, especially concerning carriage racing. To find the optimal postures, simulations were performed for driving through a curve with steady velocity and a planar floor without tilt.

In order to estimate the inertia-tensor, simplified models of the carriages are introduced. Examples of the results for a marathon and a dressage carriage are given.

Also, characteristic postures of driver and groom are identified and modelled using the mathematical model of Hanavan [6]. These identified postures are further investigated concerning variations of their inertia tensors as well as their centre of gravity depending on posture.

Finally, a dynamic model of the carriage including the humans is introduced and simulated. Results are given concerning various postures for driver and groom combinations. Special cases of dynamic behaviour like sharp cornering or the influence of acceleration are analysed as well.

Contents

| | | |
|----------|--|-----------|
| 1 | Introduction | 1 |
| 2 | Model of the carriage | 4 |
| 2.1 | Modelling approaches | 4 |
| 2.2 | Model of the front axle | 5 |
| 2.3 | Model of the marathon carriage | 6 |
| 2.4 | Model of the dressage carriage | 8 |
| 2.5 | Inertia-tensor and parallel axis theorem | 9 |
| 2.6 | Model of wheels | 11 |
| 2.6.1 | Trifilar-pendulum method | 11 |
| 2.6.2 | Calculated moment of inertia | 12 |
| 3 | Model of driver and groom | 14 |
| 3.1 | Model selection | 14 |
| 3.2 | Modelling approach | 15 |
| 3.3 | Posture of the driver | 16 |
| 3.4 | Postures of the groom on marathon carriages | 18 |
| 3.4.1 | Standing groom | 18 |
| 3.4.2 | Sitting groom | 18 |
| 3.4.2.1 | Groom sitting straight | 20 |
| 3.4.2.2 | Groom sitting and leaning | 22 |
| 3.4.2.3 | Groom sitting straight and stretching leg | 22 |
| 3.4.2.4 | Groom leaning and stretching leg | 25 |
| 3.4.2.5 | Comparison of the different sitting postures | 27 |
| 3.4.3 | Crouching groom | 27 |
| 3.5 | Posture of groom on dressage carriages | 29 |
| 4 | Dynamic system | 31 |
| 4.1 | Dynamic model with ball joint | 31 |
| 4.2 | Location of the ball joint | 34 |

| | | |
|----------|--|-----------|
| 5 | Simulation results | 36 |
| 5.1 | Marathon carriage | 36 |
| 5.1.1 | Marathon carriage with standing groom | 36 |
| 5.1.2 | Marathon carriage with sitting groom | 40 |
| 5.1.3 | Marathon carriage with crouching groom | 43 |
| 5.1.4 | Comparison of the postures | 46 |
| 5.2 | Dressage carriage | 46 |
| 5.3 | Additional simulations | 50 |
| 5.3.1 | Influence of the inertia-tensor of the carriage and humans . . . | 50 |
| 5.3.2 | Sharp cornering | 51 |
| 5.3.3 | Influence of acceleration | 53 |
| 5.3.4 | Influence of the height of the ball joint | 54 |
| 5.3.5 | Locating the ball joint in the contact point of the outer front wheel | 56 |
| 6 | Conclusion and outlook | 58 |
| | List of Figures | 60 |
| | List of Tables | 62 |
| A | Listing of the main MATLAB functions | 64 |
| B | Input data for carriage modelling | 65 |
| B.1 | Marathon carriage | 66 |
| B.2 | Dressage carriage | 67 |
| C | Input data for human modelling | 68 |
| | Bibliography | 71 |

Chapter 1

Introduction

Carriage racing can be considered a niche sport. Therefore neither carriage manufacturers nor the racing teams have the resources to closely investigate the dynamics of their vehicles and the way driver and groom can influence it. Especially when driving curves, and the groom changes position and posture in order to allow a maximum driving velocity, this lack of knowledge might lead to non optimal behaviour or mistakes that might even cause the carriage to roll over. This sort of accident causes an enormous risk of injury for both driver and groom.

The goal of this thesis is to define some guidelines for driver and groom. Which behaviour allows the highest velocities and which postures just cause high risks with rather little improvement. Therefore the maximum velocity of the carriage at tipping point will be calculated. This calculation is done for certain driver and groom combinations with different postures, positions and sizes. In figure 1.1 a racing team of the OEPS tournament in Straßwalchen-Irrsdorf of August 2015 is depicted. The groom can be seen in a typical sitting posture on a marathon carriage.

Because of racing carriages being a niche product, there is barely any literature on their dynamic behaviour. Concerning the rollover characteristics of vehicles, cars are the best analysed vehicle. Publications by Bao [1], Dong [4] and Zhang [17] for instance focus on the influence of the suspension, or crash simulation. The human body typically has a rather small mass compared to the vehicle and therefore there is no further analysis done on the human posture.

Regarding the mass distribution, driver and groom have a similar mass compared to the carriage. Considering a carriage with approximately 210 kg, and a human body with approximately 70 kg, driver and groom make 40 % of the entire system, and therefore the groom can have significant influence to the centre of gravity of the combined system. This mass distribution combined with the ability of the groom to



Figure 1.1: A racing team on a marathon carriage.

move on the rear floor of the carriage makes them rather unique.

Another aspect which has to be considered is that these carriages are usually steered with a turntable, instead of an Ackerman steering geometry that is typically found in cars. When driving through a curve, the position of the wheels relative to the carriage can change and therefore also influence the maximum velocity.

When disregarding any stabilizing effect the drawing horse might have, another aspect to consider is that a racing carriage at tipping point might behave more like a three wheeled vehicle with just one front wheel. On this topic, relevant publications can be found from Huston [9] and Van Valkenburgh [14].

The first main task of this thesis was to find and measure parameters of the carriage and apply them in order to estimate the inertia-tensor for both a marathon and dressage carriage. The chosen way of modelling as well as the calculated results are described closely in chapter 2. Also, the influence of the parallel axis theorem is discussed and the moment of inertia of a wheel was measured and compared to the selected way of modelling the wheels.

The next task was to model the main postures of driver and groom. Therefore, the main postures had to be identified and a sufficient mathematical model of the human body had to be chosen. In chapter 3 an overview of such models is given, as well as the needed data for application of the chosen model. Also, the influence of slight variations on the human posture on inertia-tensor and the location of the centre of gravity are discussed.

In chapter 4, the applied dynamic model, along with its system of equations is de-

scribed. Since this thesis deals mainly with the influence of the groom in steady state cornering, a rigid model of the carriage was chosen. Provided basic knowledge in dynamics, i.e. given by Parkus in [11], the given equations for linear and angular momentum can be derived.

The main goal of identifying the influence of the groom's posture and positioning was achieved in chapter 5. Here, all kinds of posture in different positions and for different combinations concerning the mass and size of driver and groom are given for both dressage and marathon carriages. Also, certain effects of close cornering, accelerated driving and the influence of the inertia-tensor of human and carriage are discussed as well as certain variations on the dynamic model.

In the final chapter, the calculated results are discussed and some suggestions concerning improvement on the modelling as well as on expanding the functional range of the simulation are listed.

Chapter 2

Model of the carriage

In this chapter, the considered approaches to create a model to depict the inertia-tensor based on the physical properties of the carriage are specified. The main approach was to reduce the carriage to a model based on rigid rods and/or surface-elements including a correction term. Any components which are partially carried by the horses as well as the harness are either left out or considered as rigid part of the distributed mass. Also, the wheels and front axle are modelled separately.

2.1 Modelling approaches

In order to create a feasible model of marathon and dressage carriages of all kinds without usage of CAD generated data or direct measurement of the moment and product of inertia of a carriage, the inertia-tensor can be estimated by reducing the carriage into either a general rod or plate model or by combining both. The rod model reduces the entire carriage into a simple sum of the main rods whereas the plate model depicts the carriage as a sum of its main plates. To increase precision or to consider weight differences between certain elements, an additional weighting of certain rod or plate elements can be applied.

Also, a correction mass has to be introduced, to compensate for deviation between the calculated and measured centre of gravity of the carriage. This correction mass is chosen to be a certain percentage of the mass of the carriage. If a combination of the rod and plate model is used, the mass distribution between rod and area elements has to be considered additionally.

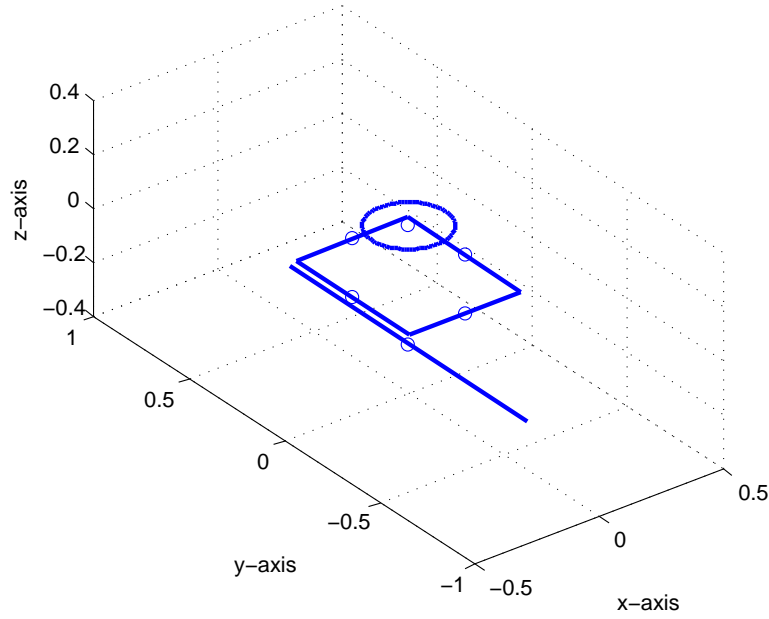


Figure 2.1: Rod model of the turntable.

2.2 Model of the front axle

Since the front axle including the turntable and suspension does have significant mass and an inertia-tensor of its own, it is modelled separately. Therefore, it is necessary to measure the mass of the entire construction of turntable, axle and suspension as well as the diameter of the turntable and the width of the axle. Also the height of the centre of gravity of the turntable from the ground has to be estimated. Using these parameters, the simplified rod model, as seen in figure 2.1, can be derived.

This model consists of rigid rods only. The circle has a diameter equivalent to that of the turntable. The lower rod has the width of the front axle and the rectangle in between consists of two rods with twice the diameter of the turntable and two rods 1.5 times the diameter. The height of the circle is equal to the height of the main floor, the height of the axle matches the measured height of the axle. Considering the estimated height of the centre of gravity, the height of the rectangle is generated accordingly. For further analysis the height of the centre of gravity was chosen to be exactly in the middle between the turntable and the axle.

Another important characteristic of this model is that the centre of gravity is within the rotational axis. Therefore, in this model, the centre of gravity of the entire carriage is independent from any rotation of the front axle.

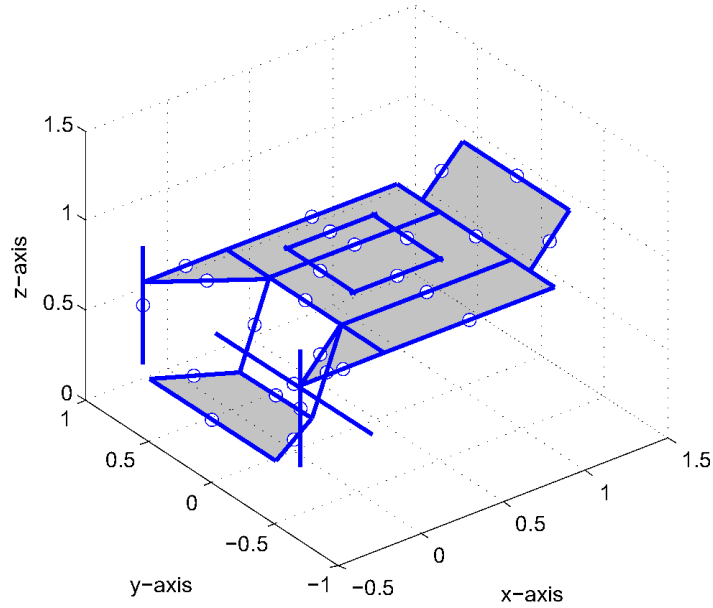


Figure 2.2: Rod and plate model of the marathon carriage.

2.3 Model of the marathon carriage

In general, a marathon carriage can be reduced to either a model of five plates or its main rods. Both kinds of model assume that the carriage is rigid and symmetrical, therefore the centre of gravity lies somewhere within its plane of symmetry.

In figure 2.2 an example of the rod and plate model is given. Here, the grey areas depict the plates which are used in the plate model, the thick lines depict all the rods that are relevant to the rod model. Despite the possibility of combining these two models as mentioned, they will now be analysed separately. For both models, the term of the correction mass was chosen to be 20 % of the mass of the carriage without the wheels and turntable.

a) The plate model:

The main advantage of the plate model is that it requires less measurements and therefore less input data. Only the inertia-tensor of five plates and the correction term in the centre of gravity needs to be calculated. Also, in order to improve the model, these five plates can be combined with individual weighting factors. For the rear trapezoid plate a weighting factor of $q_{rear} = 1.45$ was chosen, for all other plates the factor can be considered to be $q_{other} = 1$.

When using the input data from B.1 the inertia-tensor of the carriage in its centre of gravity, including the inertia-tensor of the turntable as depicted in section 2.2 and excluding the wheels, can be calculated. The resultant values are given in table 2.1.

Table 2.1: Moment and product of inertia of the area model.

| | I_{xx} | I_{yy} | I_{zz} |
|--|----------|----------|----------|
| moment of inertia in $\text{kg}\cdot\text{m}^2$ | 21.9005 | 47.4848 | 51.4100 |
| | I_{xy} | I_{xz} | I_{yz} |
| product of inertia in $\text{kg}\cdot\text{m}^2$ | 0 | -1.5125 | 0 |

b) The rod model:

This model requires more measurements, but is more feasible when applied on more complex marathon carriages. Also, it allows more flexibility when deciding what components of the carriage should or should not be part of the model. Again, individual weighting of certain rods is also possible, but so far not applied.

Using the same input data from B.1 again, the inertia-tensor of the rod model in its centre of gravity (again including the turntable but excluding the wheels) can be calculated. The resultant values are given in table 2.2.

Table 2.2: Moment and product of inertia of the rod model.

| | I_{xx} | I_{yy} | I_{zz} |
|--|----------|----------|----------|
| moment of inertia in $\text{kg}\cdot\text{m}^2$ | 26.4444 | 50.4486 | 63.0602 |
| | I_{xy} | I_{xz} | I_{yz} |
| product of inertia in $\text{kg}\cdot\text{m}^2$ | 0 | -5.5824 | 0 |

When applying a combination of these two models, the resulting inertia-tensor will lie between the values of table 2.1 and 2.2 depending on the percentage of mass that was chosen for area and rod model. In table 2.3 additional data concerning the mass distribution and centres of gravity is displayed. Here, $x_{CG,model}$ and $z_{CG,model}$ mean the centre of gravity of carriage including the turntable. The table also includes the data of the rod model of the dressage carriage, which is discussed in section 2.4.

Because the position of the correction mass of the rod model turned out to be much closer to the real centre of gravity than of the one of the area model, the area model was disregarded for further investigations. Only the rod model was applied.

Table 2.3: Additional carriage data.

| | marathon area model | marathon rod model | dressage rod model |
|-----------------|------------------------|-----------------------|-----------------------|
| m | 158.0 kg | | 228.0 kg |
| x_{CG} | 0.4700 m | | 0.6579 m |
| z_{CG} | 0.7267 m | | 0.6526 m |
| $m_{turntable}$ | 35.0 kg | | 61.0 kg |
| m_{model} | 98.4 kg | | 133.6 kg |
| $x_{CG,model}$ | 0.5409 m | 0.4426 m | 0.6359 m |
| $z_{CG,model}$ | 0.6530 m | 0.6954 m | 0.7099 m |
| m_{corr} | 24.6 kg | | 33.4 kg |
| x_{corr} | 0.0857 m | 0.6183 m | 0.7857 m |
| z_{corr} | 1.1265 m | 0.8966 m | 0.3186 m |

2.4 Model of the dressage carriage

Similarly to section 2.3, the dressage carriage model consists solely of rigid rods and a correction mass. Since the entire frame of a typical dressage carriage consists of steel beams, the additional (usually wooden) plates which are mounted on the frame are ignored. The term of the correction mass was again chosen to be 20 % of the mass of the carriage without wheels and turntable.

The respected main components of the dressage carriage are shown in figure 2.3. Also, due to different dimensions of the rods, a certain weighting factor of the mass distribution for certain rods was introduced. The main longitudinal rods were used as reference, therefore their weighting factor per length of the rod q_{other} was chosen to be 1. For the crossbeams a weighting factor of $q_{cross} = 4/3$ was chosen, since this value depicts the weight difference per length to the main rods almost exactly. Since the components of the rear suspension are not depicted in this model, the rod which represents the rear axle was included with a weighting of $q_{axle} = 7$.

When using the input data displayed in table B.2 the calculated inertia-tensor of the dressage carriage in its centre of gravity including turntable (but without the wheels) can be calculated. Table 2.4 shows the resultant values.

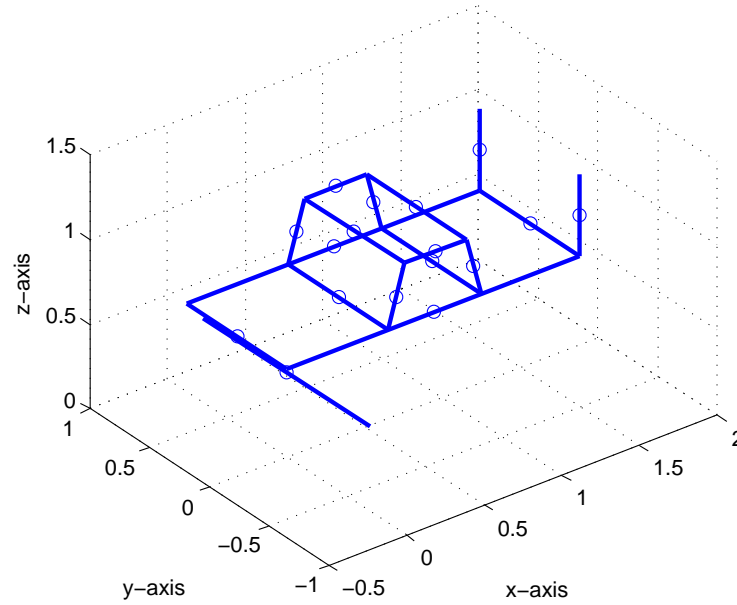


Figure 2.3: Rod model of the dressage carriage.

Table 2.4: Moment and product of inertia of the rod model of a dressage carriage.

| | I_{xx} | I_{yy} | I_{zz} |
|--|----------|----------|----------|
| moment of inertia in $\text{kg}\cdot\text{m}^2$ | 39.0865 | 80.7192 | 90.0641 |
| | I_{xy} | I_{xz} | I_{yz} |
| product of inertia in $\text{kg}\cdot\text{m}^2$ | 0 | -4.4881 | 0 |

2.5 Inertia-tensor and parallel axis theorem

During cornering the centre of rotation is not the centre of gravity of the carriage. So the parallel axis theorem has to be applied. The influence of the parallel axis theorem will be discussed using a simple example. For this purpose the rotation of the turntable, and the change of the inertia-tensor that comes with it, is disregarded. The reference-point for the inertia-tensor is only varied along the y-axis, the distances of x and z are considered constant. The angular velocity during cornering is considered to be $\vec{\omega} = (0 \ 0 \ \omega)^T$. Therefore only the third column of the tensor is relevant.

For a given inertia-tensor, divided by the mass of the rigid body and the centre of

Table 2.5: Influence of parallel axis theorem.

| | m in kg | x in m | z in m | $\frac{I_{CGxz}}{m}$ in m ² | $\frac{I_{CGzz}}{m}$ in m ² |
|-------------------|-----------|----------|----------|--|--|
| marathon carriage | 158 | 0.470 | 0.727 | -0.0353 | 0.3991 |
| dressage carriage | 228 | 0.658 | 0.653 | -0.0197 | 0.3950 |

| | y_{ICGzz} in m | $-xz$ in m ² | $-yz _{y=2}$ in m ² | $x^2 + y^2 _{y=2}$ in m ² |
|-------------------|------------------|-------------------------|--------------------------------|--------------------------------------|
| marathon carriage | 0.632 | -0.3416 | -1.4534 | 4.2209 |
| dressage carriage | 0.629 | -0.4294 | -1.3052 | 4.4328 |

gravity being $\vec{r}_{CG} = (x \ y \ z)^T$, the inertia-tensor with respect to the point O $(0 \ 0 \ 0)^T$ can be calculated by

$$\frac{\mathbf{I}_0}{m} = \frac{\mathbf{I}_{CG}}{m} + \begin{pmatrix} y^2 + z^2 & -xy & -xz \\ -xy & x^2 + z^2 & -yz \\ -xz & -yz & x^2 + y^2 \end{pmatrix}. \quad (2.1)$$

As seen in equation 2.1, the product of inertia and moment of inertia are partially sensitive to the distance between the centre of gravity and the rotational axis in O. The component I_{xz} does not vary with different y -values, because it's changes are only dependent on the x - and z -values. And I_{yz} is linearly dependent on variations in y . The component I_{zz} is very sensitive to y , because of y^2 .

In table 2.5, the relevant carriage data and results of the parallel axis theorem are presented. Here, y_{ICGzz} is the length where the moment of inertia added due to the parallel axis theorem is equal to the moment of inertia in the centre of gravity.

Because of the symmetry of the carriages, the product of inertia $I_{CGyz} = 0$ for both, meaning that I_{0yz} is only caused by the parallel axis theorem. I_{CGxz} and I_{0xz} are only depending on the geometric properties of the carriage, but most of the product of inertia I_{0xz} is caused by the parallel axis theorem. For the marathon carriage it is 91 % and for the dressage carriage it is 96 %.

The moment of inertia I_{0zz} is mostly influenced by the cornering radius. In the given table the moment of inertia per mass for a curve with 2m radius is given, here, for the marathon carriage the moment of inertia is 91 % caused by the parallel axis theorem. For the dressage carriage it is 92 %.

2.6 Model of wheels

In order to consider the dynamic influence of the rotation of the wheels on the maximum velocity, they can be modelled as a combination of a thick-walled cylindrical tube and a solid cylinder. For validation a wheel of the "Kühnle" marathon carriage was weighted and its moment of inertia was determined using the trifilar-pendulum method [8]. The main characteristics of this wheel are

$$m_W = 11.5 \text{ kg} \quad d_W = 0.748 \text{ m} \Rightarrow r_W = 0.374 \text{ m} \quad w_W = 0.04 \text{ m},$$

with m_W being the mass of the entire wheel (including brake disc), d_W being its outer diameter and w_W being its outer width.

2.6.1 Trifilar-pendulum method

Table 2.6: Measured data including estimated errors.

| | unit | value | absolute error | relative error in % |
|-----------------------|----------------------|-------|----------------|---------------------|
| period of oscillation | $[T] = \text{s}$ | 57.50 | ± 0.2 | $\tau_T = 0.35$ |
| mass | $[m] = \text{kg}$ | 11.5 | ± 0.1 | $\tau_m = 0.87$ |
| gravity constant | $[g] = \text{m/s}^2$ | 9.81 | ± 0.05 | $\tau_g = 0.51$ |
| length of triangle | $[a_H] = \text{m}$ | 0.58 | ± 0.005 | $\tau_a = 0.87$ |
| length of wire | $[l_H] = \text{m}$ | 2.88 | ± 0.01 | $\tau_l = 0.35$ |

The trifilar-pendulum method allows to measure the moment of inertia with the period of rotational oscillation. The moment of inertia (the rotational axis is the y axis) is calculated with

$$I_{yy} = \frac{\bar{T}^2 m g r_H^2}{4 \pi^2 l_H}. \quad (2.2)$$

The additionally needed data for applying the trifilar-method [8] is given in table 2.6 and the measured durations of twenty periods (repeated five times) in s are

$$T_{20} = \{57.6, 57.51, 57.62, 57.31, 57.45\}.$$

In table 2.6, g means the acceleration due to gravitation, $r_H = 0.3325 \text{ m}$ is the distance from the centre of the wheel to any wire, a_H is the length of a side of the equilateral triangle of the wires and l_H is the length of the suspending wires. Given the values of T_{20} for 20 oscillations, the average duration of one period is $\bar{T} = 2.8749 \text{ s}$.

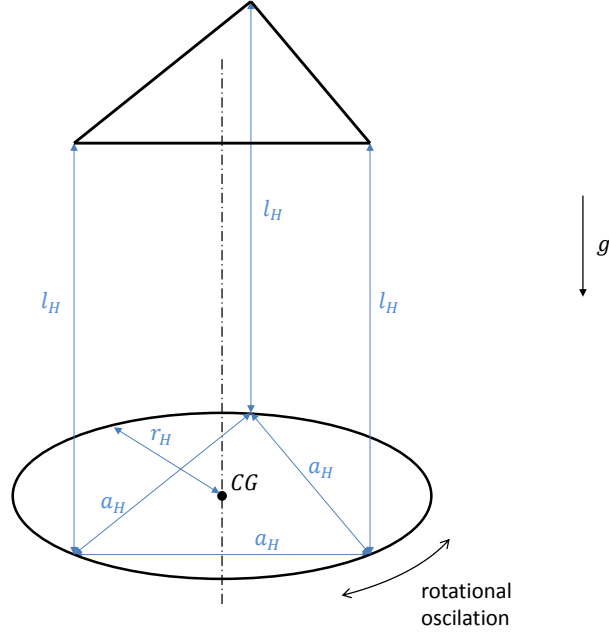


Figure 2.4: Draft of the geometry for applying the trifilar pendulum method.

Table 2.7: Calculated moment of inertia of wheels.

| | m in kg | d_W in m | w in m | $I_{xx} = I_{zz}$ in $\text{kg}\cdot\text{m}^2$ | I_{yy} in $\text{kg}\cdot\text{m}^2$ |
|----------------------|-----------|------------|----------|--|---|
| marathon wheel | 11.5 | 0.748 | 0.040 | 0.4505 | 0.8980 |
| dressage front wheel | 13.5 | 0.795 | 0.045 | 0.5977 | 1.1908 |
| dressage rear wheel | 19.5 | 0.994 | 0.045 | 1.3478 | 2.6890 |

With the given parameters the moment of inertia is

$$I_{yy} = 0.906\,97\,\text{kg}\cdot\text{m}^2. \quad (2.3)$$

Considering the data from table 2.6, the expected error results to be

$$\tau = 2.15\,\%. \quad (2.4)$$

2.6.2 Calculated moment of inertia

In order to calculate the moment of inertia of the wheel from a model in a way that fits the result of section 2.6.1, it is considered as a combination of a a thick-walled

cylindrical outer tube and a solid inner cylinder. With the measured mass, diameter and width of the wheel, the moment of inertia can be modelled.

The needed diameters to calculate the moment of inertia are chosen as portions of the wheel radius $r_W = d_W/2$. For the outer ring the used radii are

$$r_{2out} = r_W \quad r_{1out} = 0.9 r_W \quad (2.5)$$

and for the inner cylinder it is

$$r_{in} = 0.25 r_W. \quad (2.6)$$

Additionally, when distributing the mass between these two bodies, the inner cylinder was considered to have twice the density of mass of the outer tube. Given the equations to calculate the moment of inertia of thick-walled cylindrical tubes and solid cylinders

$$I_{yy,tube} = \frac{m_{tube}}{2} (r_{2,tube}^2 + r_{1,tube}^2) \quad (2.7)$$

$$I_{yy,cyl} = \frac{m_{cyl} r_{cyl}^2}{2} \quad (2.8)$$

which can be found i.e. in [13], the moment of inertia can be calculated.

In table 2.7, the input data and resulting moment of inertia for the measured dressage and marathon carriage are given. In comparison, for a solid cylinder with the data from 2.6, the moment of inertia would be $I_{yy} = 0.8043 \text{ kg}\cdot\text{m}^2$.

Now, comparing the result of the previous chapter shows, that the calculated moment of inertia I_{yy} for the wheel of the marathon carriage is very close to the measured value. However, since the moment of inertia along the a radial axis could not be measured, the same precision cannot be assumed for the calculated moment of inertia $I_{xx} = I_{zz}$.

Chapter 3

Model of driver and groom

This chapter deals with modelling of the human body to generate the inertia-tensors of driver and groom as well as with the identification of the typical postures during racing.

3.1 Model selection

In order to estimate the inertia-tensor of the human body, numerous mathematical models have been developed since the late 1950s and early 1960s. One of the first widely used models was developed by Hanavan [6] in 1964. The human body was divided into 15 segments and modelled with simple geometric solids. For validation it was compared with results presented by Santschi [12]. Before that, in 1963, Whitsett [15] presented a very similar mathematical model, with only one solid for the entire torso. The properties as well as the dimension of these segments can be calculated via anthropometric data of individual subjects.

Another study concerning the estimation of the inertia-tensor of body segments was done by Clauser [3] in 1969. Here, the human body was divided into 14 segments and another method to calculate the inertia-tensor and centre of mass was applied. Another study was presented by Chandler et al. [2] in 1975, as well as one of the early computer multi body system models by Fleck and Butler [5].

All these mentioned studies were developed at the Aerospace Research Laboratory at the Wright-Patterson Air Force Base in Ohio. Back then, developing and validating models had a high priority for early developments in space flight. Another main driving force of research of the dynamic behaviour of the human body was the development and improvement of car safety.

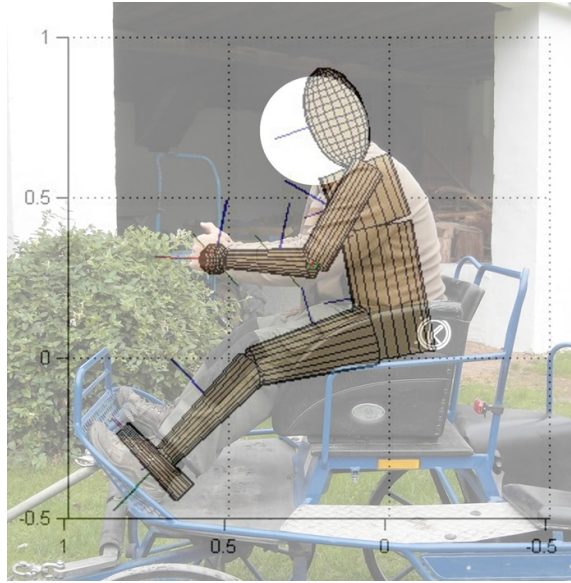


Figure 3.1: Overlap of sitting driver and positioned p75 dummy.

Later work in the field of modelling the human body was published among others by Hatze [7] and Yeadon [16], but the modelling approach remained merely the same as in the early publications. The human body is still reduced to certain solid segments, only the geometric detail and number of segments is increased.

The model chosen for further analysis is based on Hanavan [6], including the anthropometric data published alongside with his model. There, the measurements of human bodies were categorized in groups of a certain percentile of the "air force men", meaning that for example a 50-percentile human is an air force man where 50 % of the measured subjects have smaller values for weight, height, etc. and 50 % have higher values. This model is accurate enough, simple in the implementation and it is still used in similar publications (i.e. [10]) up until today.

3.2 Modelling approach

In order to recreate typical postures of driver and groom, pictures of a person sitting in the identified positions were required. These pictures, along with certain measurements of the carriage were compared with the position of a virtual Hanavan "dummy".

In sections 3.3 to 3.5, the postures were generated using a 75-percentile Hanavan model.

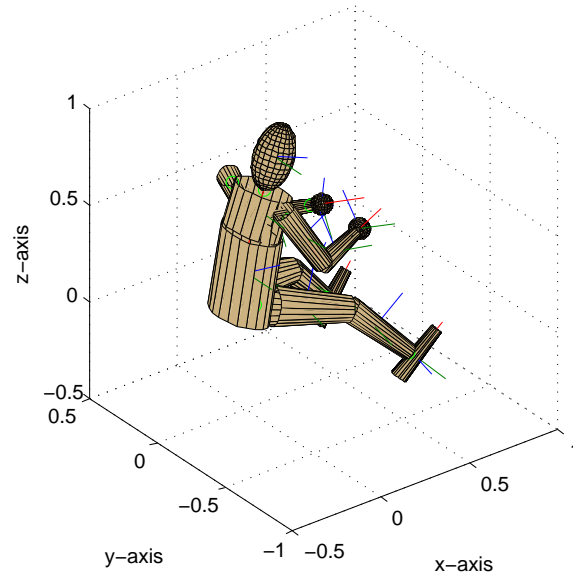


Figure 3.2: Posture of the p75-dummy as driver.

In figure 3.1 an example for comparing the posture of a human driver and a 75-percentile Hanavan model (referred to as "p75-dummy") is given. This picture comparison combined with measurements of carriage and locations of components of the Hanavan model is a feasible way to generate all kinds of positions for the virtual dummies.

In order to compare different kinds of drivers and grooms, an additional p50 and p25 dummy was generated. The masses of the dummies are $m_{p25} = 67.44$ kg, $m_{p50} = 73.43$ kg and $m_{p75} = 80.10$ kg. For comparability, the joint angles of every posture were kept the same, but the rotation of the entire dummy was varied for different drivers.

3.3 Posture of the driver

In table C.1, the chosen values for the joint angles (in deg) for a sitting driver are shown. The centre of the coordinates was chosen to be the central sitting point. Since the centre of the coordinates at $cm3 = (0\ 0\ 0)^T$ equals the centre of segment 3 (the lower body), the value depicted in table C.1 moves the model upwards for half the length of the segment 3, the lower torso. In figure 3.2, the resulting posture using the input data from table C.1 is displayed.

Table 3.1: Moment and product of inertia as well as the centre of gravity of the driver.

| | Components of inertia tensor $[I] = \text{kg}\cdot\text{m}^2$ | | | Centre of gravity $[\vec{r}_{CG}] = \text{m}$ | | |
|-----|--|----------|----------|--|----------|----------|
| | I_{xz} | I_{yz} | I_{zz} | x_{CG} | y_{CG} | z_{CG} |
| p25 | 1.5840 | 0.0052 | 2.9962 | 0.1589 | 0 | 0.1981 |
| p50 | 1.8698 | 0.0059 | 3.5544 | 0.1651 | 0 | 0.2111 |
| p75 | 2.2163 | 0.0066 | 5.3144 | 0.1703 | 0 | 0.2220 |

Table 3.2: Ranges for the values of moment and product of inertia as well as position of the centre of gravity of the driver.

| | Components of inertia tensor $[I] = \text{kg}\cdot\text{m}^2$ | | | Centre of gravity $[\vec{r}_{CG}] = \text{m}$ | | |
|--------------------|--|----------|----------|--|----------|----------|
| | I_{xz} | I_{yz} | I_{zz} | x_{CG} | y_{CG} | z_{CG} |
| p25 _{min} | 1.6072 | -0.4013 | 2.9465 | 0.1544 | -0.0122 | 0.1985 |
| p25 _{max} | 1.6792 | 0.3292 | 2.8833 | 0.1547 | 0.0118 | 0.1931 |
| p50 _{min} | 1.7213 | -0.3647 | 3.6150 | 0.1683 | -0.0055 | 0.2076 |
| p50 _{max} | 2.0307 | 0.2625 | 3.5695 | 0.1602 | 0.0003 | 0.2120 |
| p75 _{min} | 2.1418 | -0.3433 | 5.1771 | 0.1744 | -0.0081 | 0.2187 |
| p75 _{max} | 2.2932 | 0.5223 | 5.3603 | 0.1678 | 0.0036 | 0.2276 |

The relevant data for further calculations is shown in table 3.1. Also, values for slight variations of the joint angles are shown in table 3.2. To generate these results, each joint was given a random deviation of ± 5 deg. From hundred random results those with the highest and lowest value for $I_{xz} + I_{yz}$ were selected. The same criteria was applied for all other dummy postures.

The variation of the centre of gravity of the p50-driver stays within a distance of less than 1 cm. The difference in the moment of inertia I_{zz} is about $0.0606 \text{ kg}\cdot\text{m}^2$ and the difference in the product of inertia I_{xz} and I_{yz} stays within $0.3705 \text{ kg}\cdot\text{m}^2$.

3.4 Postures of the groom on marathon carriages

In the following, various postures of the groom are analysed. The three main postures of the groom on a marathon carriage are standing, sitting and crouching. Additionally, four different variations of the sitting posture are considered.

3.4.1 Standing groom

One of the most typical postures of the groom is standing on the rear floor of the carriage. In table C.2, the corresponding joint angles are shown. The model was shifted so, that the origin of the coordinate-system is placed between the center of gravity of the right and left foot and the z -axis is oriented in the direction of the z -axis of the lower torso segment. In figure 3.3, the resulting posture using the shown input data is displayed.

The relevant data for further calculations is shown in table 3.3. Again, values for slight variations of the joint angles within ± 5 deg are shown in table 3.4. The results for the variations of the position were chosen just like in section 3.3.

Comparing the data reveals that the variation of the centre of gravity of the standing p50-groom stays within a distance of 1.02 cm, the difference of the moment of inertia I_{zz} is about $0.0829 \text{ kg}\cdot\text{m}^2$ and the difference of the product of inertia I_{xz} and I_{yz} stays within $0.4915 \text{ kg}\cdot\text{m}^2$.

3.4.2 Sitting groom

Here, four different sitting postures for left turn curves are discussed: the groom sitting straight, the groom leaning out of the carriage and the groom stretching the

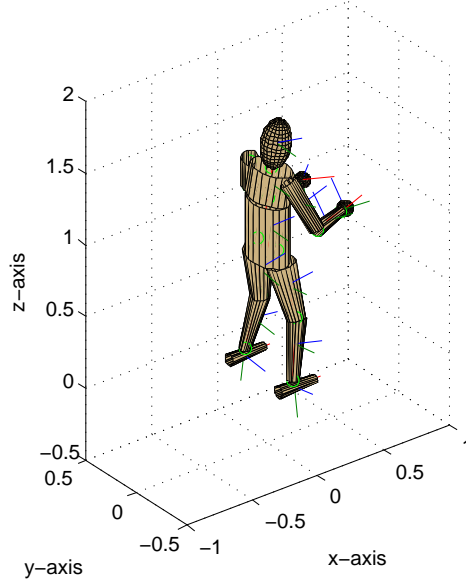


Figure 3.3: Posture of the p75-dummy as standing groom.

Table 3.3: Moment and product of inertia as well as the centre of gravity of the standing groom.

| | Components of inertia tensor $[I] = \text{kg} \cdot \text{m}^2$ | | | Centre of gravity $[\vec{r}_{CG}] = \text{m}$ | | |
|-----|--|----------|----------|--|----------|----------|
| | I_{xz} | I_{yz} | I_{zz} | x_{CG} | y_{CG} | z_{CG} |
| p25 | -0.0718 | 0 | 1.6758 | 0.0381 | 0 | 0.8858 |
| p50 | -0.0849 | 0 | 1.9887 | 0.0394 | 0 | 0.9088 |
| p75 | -0.0833 | 0 | 2.3512 | 0.0403 | 0 | 0.9305 |

Table 3.4: Ranges for the values of moment and product of inertia as well as position of the centre of gravity of the standing groom.

| | Components of inertia tensor $[I] = \text{kg} \cdot \text{m}^2$ | | | Centre of gravity $[\vec{r}_{CG}] = \text{m}$ | | |
|--------------------|--|----------|----------|--|----------|----------|
| | I_{xz} | I_{yz} | I_{zz} | x_{CG} | y_{CG} | z_{CG} |
| p25 _{min} | -0.4178 | -0.2258 | 1.5657 | 0.0244 | 0 | 0.8846 |
| p25 _{max} | 0.2389 | 0.2861 | 1.5940 | 0.0469 | 0.0035 | 0.8849 |
| p50 _{min} | -0.5648 | -0.4336 | 2.0715 | 0.0312 | -0.0059 | 0.9089 |
| p50 _{max} | 0.3332 | 0.4915 | 2.0164 | 0.0426 | 0.0080 | 0.9115 |
| p75 _{min} | -0.5453 | -1.1975 | 2.5383 | 0.0379 | -0.0085 | 0.9295 |
| p75 _{max} | 0.1479 | 0.5766 | 2.4040 | 0.0394 | 0.0078 | 0.9320 |

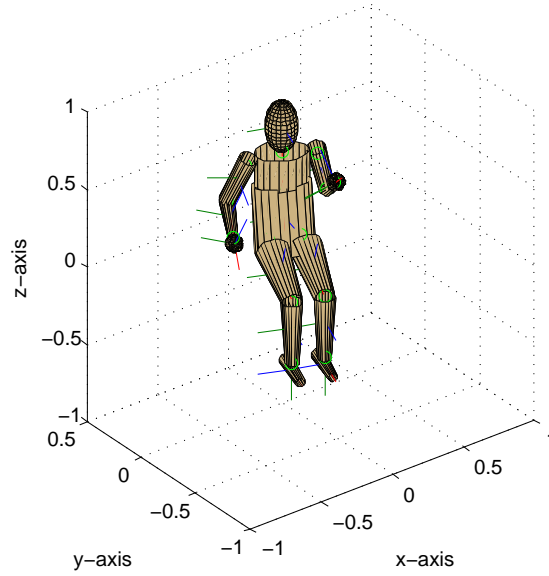


Figure 3.4: Posture of the p75-dummy as straight sitting groom.

left leg (i.e. in order to have better hold on the carriage) for both the sitting and leaning posture.

3.4.2.1 Groom sitting straight

The chosen values for the joint angles are given in table C.3. Here the origin of the coordinates was again chosen to be the sitting point, just like it was chosen for the driver in section 3.3. The resulting posture, using the given input data, can be seen in figure 3.4.

Table 3.5 displays the relevant data. Values for slight variations of the joint angles within ± 5 deg are shown in table 3.6.

The variation of the centre of gravity of the standing p50-groom stays within a distance of 1.5 cm and the difference of the moment of inertia I_{zz} is about $0.1219 \text{ kg}\cdot\text{m}^2$ and the difference of the product of inertia I_{xz} and I_{yz} stays within $0.3763 \text{ kg}\cdot\text{m}^2$.

Table 3.5: Moment and product of inertia as well as the centre of gravity of the groom sitting straight.

| | Components of inertia tensor $[I] = \text{kg}\cdot\text{m}^2$ | | | Centre of gravity $[\vec{r}_{CG}] = \text{m}$ | | |
|-----|--|----------|----------|--|----------|----------|
| | I_{xz} | I_{yz} | I_{zz} | x_{CG} | y_{CG} | z_{CG} |
| p25 | -0.9421 | -2.5649 | 3.0430 | -0.0338 | -0.0894 | 0.1886 |
| p50 | -1.0866 | -2.9489 | 3.5581 | -0.0394 | -0.0924 | 0.1984 |
| p75 | -1.2452 | -3.3697 | 4.1598 | -0.0361 | -0.0956 | 0.2057 |

Table 3.6: Ranges for the values of moment and product of inertia as well as position of the centre of gravity of the straight sitting groom.

| | Components of inertia tensor $[I] = \text{kg}\cdot\text{m}^2$ | | | Centre of gravity $[\vec{r}_{CG}] = \text{m}$ | | |
|--------------------|--|----------|----------|--|----------|----------|
| | I_{xz} | I_{yz} | I_{zz} | x_{CG} | y_{CG} | z_{CG} |
| p25 _{min} | -1.2162 | -2.6244 | 3.1507 | -0.0393 | -0.0837 | 0.1855 |
| p25 _{max} | -0.6814 | -2.5422 | 3.0758 | -0.0318 | -0.0902 | 0.1874 |
| p50 _{min} | -1.3378 | -3.0080 | 3.5084 | -0.0440 | -0.0821 | 0.1940 |
| p50 _{max} | -0.7103 | -2.9400 | 3.4362 | -0.0271 | -0.0965 | 0.1971 |
| p75 _{min} | -1.3296 | -3.5310 | 4.3981 | -0.0316 | -0.0961 | 0.2097 |
| p75 _{max} | -0.9040 | -3.2117 | 3.8335 | -0.0326 | -0.0951 | 0.1994 |

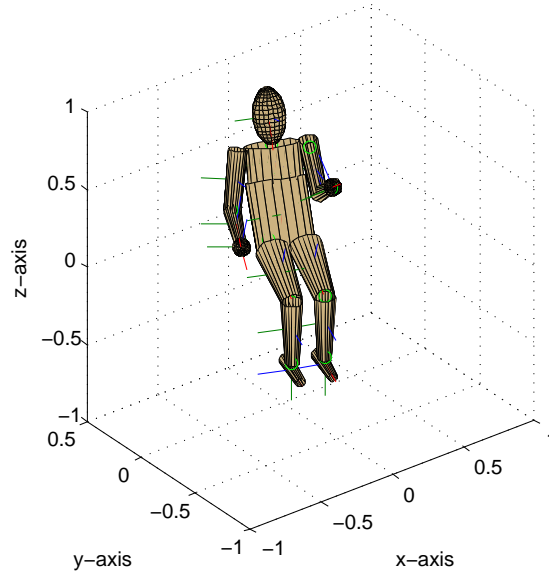


Figure 3.5: Posture of the p75-dummy as leaning groom.

3.4.2.2 Groom sitting and leaning

The chosen values for the joint angles are given in table C.3. Shifting and rotating the model has to be done in a way that the legs keep the same position as for the straight sitting groom. The resulting posture, using the given input data, can be seen in figure 3.5.

Table 3.7 shows the resulting data. Values for slight variations of the joint angles within ± 5 deg are shown in table 3.8.

The variation of the centre of gravity of the standing p50-groom stays within a distance of less than 1 cm. The difference of the moment of inertia I_{zz} is about $0.2683 \text{ kg}\cdot\text{m}^2$ and the maximum difference of the product of inertia I_{xz} and I_{yz} is about $0.3432 \text{ kg}\cdot\text{m}^2$.

3.4.2.3 Groom sitting straight and stretching leg

This virtual dummy is modelled much like the sitting groom. Except for the angle of the lower left leg, the chosen values for the joint angles given in table C.5 are the same as in table C.3. The centre of the coordinates was chosen again to be the sitting point. The resulting posture, can be seen in figure 3.6.

Table 3.7: Moment and product of inertia as well as the centre of gravity of the groom leaning.

| | Components of inertia tensor $[I] = \text{kg} \cdot \text{m}^2$ | | | Centre of gravity $[\vec{r}_{CG}] = \text{m}$ | | |
|-----|--|----------|----------|--|----------|----------|
| | I_{xz} | I_{yz} | I_{zz} | x_{CG} | y_{CG} | z_{CG} |
| p25 | -1.1794 | -3.3813 | 4.2776 | -0.0136 | -0.0354 | 0.1673 |
| p50 | -1.3549 | -3.8779 | 4.9646 | -0.0146 | -0.0378 | 0.1768 |
| p75 | -1.5416 | -4.4062 | 5.7412 | -0.0159 | -0.0413 | 0.1841 |

Table 3.8: Ranges for the values of moment and product of inertia as well as position of the centre of gravity of the leaning groom.

| | Components of inertia tensor $[I] = \text{kg} \cdot \text{m}^2$ | | | Centre of gravity $[\vec{r}_{CG}] = \text{m}$ | | |
|--------------------|--|----------|----------|--|----------|----------|
| | I_{xz} | I_{yz} | I_{zz} | x_{CG} | y_{CG} | z_{CG} |
| p25 _{min} | -1.4210 | -3.3823 | 4.4834 | -0.0193 | -0.0337 | 0.1695 |
| p25 _{max} | -0.9069 | -3.3659 | 3.9243 | -0.0058 | -0.0355 | 0.1622 |
| p50 _{min} | -1.6614 | -3.8588 | 5.2328 | -0.0168 | -0.0334 | 0.1752 |
| p50 _{max} | -1.0118 | -3.8454 | 4.7827 | -0.0103 | -0.0432 | 0.1791 |
| p75 _{min} | -1.8247 | -4.4684 | 5.9282 | -0.0217 | -0.0356 | 0.1801 |
| p75 _{max} | -1.2275 | -4.4185 | 5.6986 | -0.0134 | -0.0422 | 0.1835 |

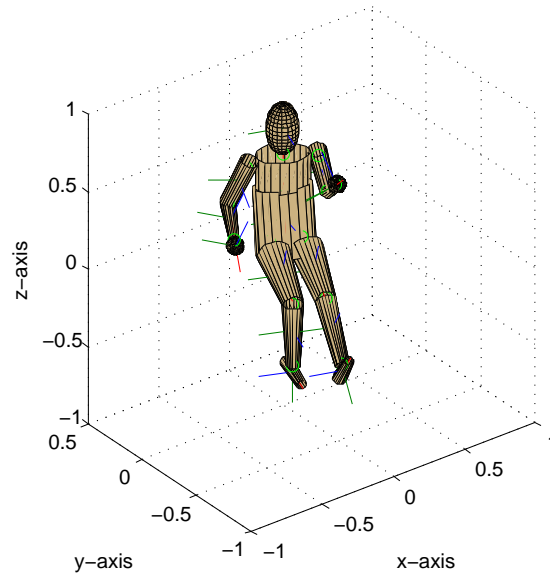


Figure 3.6: Posture of the p75-dummy as sitting groom with stretched leg.

Table 3.9: Moment and product of inertia as well as the centre of gravity of the sitting groom with stretched leg.

| | Components of inertia tensor $[I] = \text{kg}\cdot\text{m}^2$ | | | Centre of gravity $[\vec{r}_{CG}] = \text{m}$ | | |
|-----|--|----------|----------|--|----------|----------|
| | I_{xz} | I_{yz} | I_{zz} | x_{CG} | y_{CG} | z_{CG} |
| p25 | -1.0236 | -2.7473 | 3.6958 | -0.0374 | -0.0994 | 0.1936 |
| p50 | -1.1804 | -3.1573 | 4.3119 | -0.0386 | -0.1027 | 0.2035 |
| p75 | -1.3530 | -3.6068 | 5.0319 | -0.0400 | -0.1063 | 0.2110 |

Table 3.10: Ranges for the values of moment and product of inertia as well as position of the centre of gravity of the sitting groom with stretched leg.

| | Components of inertia tensor $[I] = \text{kg}\cdot\text{m}^2$ | | | Centre of gravity $[\vec{r}_{CG}] = \text{m}$ | | |
|--------------------|--|----------|----------|--|----------|----------|
| | I_{xz} | I_{yz} | I_{zz} | x_{CG} | y_{CG} | z_{CG} |
| p25 _{min} | -1.4035 | -2.6452 | 3.8069 | -0.0477 | -0.0951 | 0.1952 |
| p25 _{max} | -0.7037 | -2.7465 | 3.6436 | -0.0297 | -0.0994 | 0.1924 |
| p50 _{min} | -1.5884 | -3.1136 | 4.3168 | -0.0515 | -0.0934 | 0.2010 |
| p50 _{max} | -0.9506 | -3.0423 | 4.3194 | -0.0375 | -0.1044 | 0.2033 |
| p75 _{min} | -1.6266 | -3.6589 | 5.1709 | -0.0447 | -0.1018 | 0.2107 |
| p75 _{max} | -1.0023 | -3.5660 | 4.8443 | -0.0341 | -0.1071 | 0.2058 |

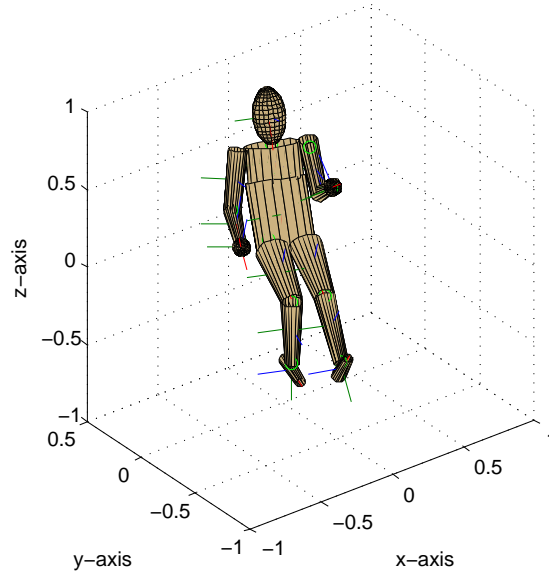


Figure 3.7: Posture of the p75-dummy as leaning groom with stretched leg.

Table 3.9 again displays the resultant data. Values for slight variations of the joint angles within ± 5 deg are shown in table 3.10.

The variation of the centre of gravity of the standing p50-groom is 1.6 cm and the difference of the moment of inertia I_{zz} is about $0.4080 \text{ kg}\cdot\text{m}^2$ and the difference of the product of inertia I_{xz} and I_{yz} stays within $0.2299 \text{ kg}\cdot\text{m}^2$.

3.4.2.4 Groom leaning and stretching leg

This model is similar to the leaning groom. The difference of the joint angles between table C.5 and table C.6 is in the angle of the lower left leg. The same centre of coordinates was chosen as for the normal leaning groom. The resulting posture can be seen in figure 3.7.

Table 3.11 shows the resultant data. Values for slight variations of the joint angles within ± 5 deg are shown in table 3.12.

The variation of the centre of gravity of the standing p50-groom is about 1.2 cm and the difference of the moment of inertia I_{zz} is about $0.1183 \text{ kg}\cdot\text{m}^2$ and the maximum difference of the product of inertia I_{xz} and I_{yz} is about $0.3730 \text{ kg}\cdot\text{m}^2$.

Table 3.11: Moment and product of inertia as well as the centre of gravity of the leaning groom with stretched leg.

| | Components of inertia tensor $[I] = \text{kg}\cdot\text{m}^2$ | | | Centre of gravity $[\vec{r}_{CG}] = \text{m}$ | | |
|-----|--|----------|----------|--|----------|----------|
| | I_{xz} | I_{yz} | I_{zz} | x_{CG} | y_{CG} | z_{CG} |
| p25 | -1.2490 | -3.5314 | 5.0131 | -0.0173 | -0.0454 | 0.1722 |
| p50 | -1.4352 | -4.0494 | 5.8123 | -0.0184 | -0.0482 | 0.1819 |
| p75 | -1.6340 | -4.6017 | 6.7192 | -0.0198 | -0.0520 | 0.1895 |

Table 3.12: Ranges for the values of moment and product of inertia as well as position of the centre of gravity of the leaning groom with stretched leg.

| | Components of inertia tensor $[I] = \text{kg}\cdot\text{m}^2$ | | | Centre of gravity $[\vec{r}_{CG}] = \text{m}$ | | |
|--------------------|--|----------|----------|--|----------|----------|
| | I_{xz} | I_{yz} | I_{zz} | x_{CG} | y_{CG} | z_{CG} |
| p25 _{min} | -1.5400 | -3.4791 | 4.9067 | -0.0298 | -0.0395 | 0.1698 |
| p25 _{max} | -1.0491 | -3.4145 | 4.8619 | -0.0064 | -0.0486 | 0.1731 |
| p50 _{min} | -1.6346 | -4.1525 | 5.7744 | -0.0256 | -0.0412 | 0.1777 |
| p50 _{max} | -1.0622 | -4.1220 | 5.6940 | -0.0067 | -0.0519 | 0.1814 |
| p75 _{min} | -1.8564 | -4.7204 | 6.6980 | -0.0279 | -0.0426 | 0.1833 |
| p75 _{max} | -1.2643 | -4.6040 | 6.5159 | -0.0115 | -0.0560 | 0.1886 |

3.4.2.5 Comparison of the different sitting postures

In order to clarify if and how much the sitting groom can change his or her own centre of gravity and inertia tensor, the above mentioned postures will be discussed. Obviously, the main goal of the groom is to bring the centre of gravity closer to the centre of curvature of the path driven and as low as possible.

Considering the strong influence of the parallel axis theorem, the different locations of the centre of gravity play an important role. Especially the y -component, which is oriented towards the centre of curvature. Keeping in mind that all the Hanavan dummies were modelled for left turns, the largest value for \vec{r}_{CGy} is considered the best.

For p50-dummies, the posture with both the greatest \vec{r}_{CGy} and lowest \vec{r}_{CGz} is the leaning groom without stretching the left leg. On the other hand, the least favourable seating posture is the straight sitting groom with the stretched lower leg. It is also worth mentioning that the difference of the location of the centre of gravity of these two postures is just 1.7 cm and that the leaning posture comes with a higher risk for the groom to fall off the carriage.

3.4.3 Crouching groom

The groom crouches on the rear floor of the carriage. The values for the joint angles are shown in table C.7. The dummy was shifted so, that the origin of the coordinates was chosen to be the in between the centre of gravity of the left and right foot. In figure 3.8, the resulting posture is displayed. Of all postures, this one has the lowest centre of gravity, but due to the geometry of the carriage the groom is limited in the ability to move to the side.

The relevant data for further calculations is shown in table 3.13. Values for slight variations of the joint angles within $\pm 5^\circ$ are shown in table 3.14.

The variation of the centre of gravity of the standing p50-groom stays within a distance of 1.12 cm and the difference of the moment of inertia I_{zz} is about $0.0487 \text{ kg}\cdot\text{m}^2$ and the difference of the product of inertia I_{xz} and I_{yz} is about $0.2293 \text{ kg}\cdot\text{m}^2$.

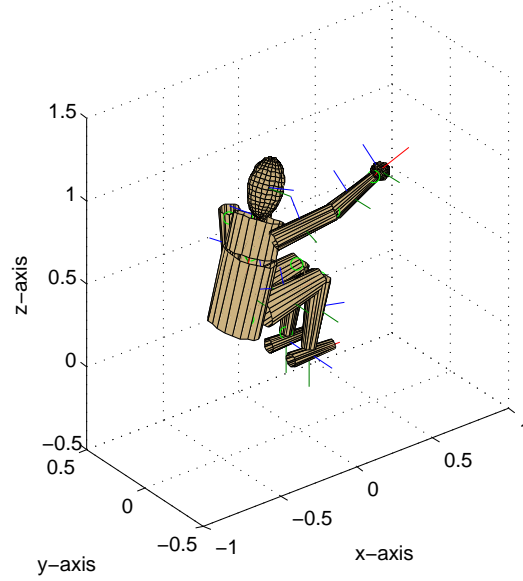


Figure 3.8: Posture of the p75-dummy as crouching groom.

Table 3.13: Moment and product of inertia as well as the centre of gravity of the crouching groom.

| | Components of inertia tensor $[I] = \text{kg} \cdot \text{m}^2$ | | | Centre of gravity $[\vec{r}_{CG}] = \text{m}$ | | |
|-----|--|----------|----------|--|----------|----------|
| | I_{xz} | I_{yz} | I_{zz} | x_{CG} | y_{CG} | z_{CG} |
| p25 | 0.0255 | 0.0595 | 2.3461 | -0.1996 | 0.0060 | 0.5057 |
| p50 | 0.0281 | 0.0770 | 2.7522 | -0.2045 | 0.0062 | 0.5194 |
| p75 | 0.0588 | 0.1033 | 3.2224 | -0.2105 | 0.0061 | 0.5320 |

Table 3.14: Ranges for the values of moment and product of inertia as well as position of the centre of gravity of the crouching groom.

| | Components of inertia tensor $[I] = \text{kg} \cdot \text{m}^2$ | | | Centre of gravity $[\vec{r}_{CG}] = \text{m}$ | | |
|--------------------|--|----------|----------|--|----------|----------|
| | I_{xz} | I_{yz} | I_{zz} | x_{CG} | y_{CG} | z_{CG} |
| p25 _{min} | -0.0540 | -0.1645 | 2.2631 | -0.1997 | 0.0014 | 0.5032 |
| p25 _{max} | 0.1008 | 0.2786 | 2.3206 | -0.2055 | 0.0163 | 0.5039 |
| p50 _{min} | -0.0938 | -0.1263 | 2.7034 | -0.2023 | 0.0069 | 0.5178 |
| p50 _{max} | 0.0941 | 0.3063 | 2.7420 | -0.2070 | 0.0165 | 0.5156 |
| p75 _{min} | -0.0724 | -0.1332 | 3.1870 | -0.2082 | 0.0125 | 0.5358 |
| p75 _{max} | 0.2491 | 0.3935 | 3.2323 | -0.2151 | 0.0062 | 0.5330 |

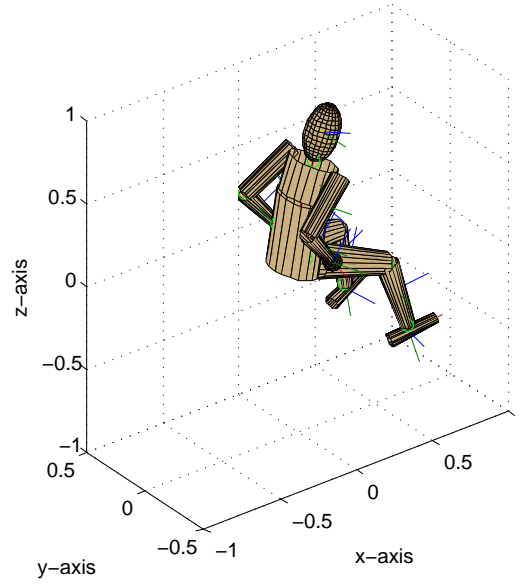


Figure 3.9: Posture of the p75-dummy as groom on dressage carriage.

3.5 Posture of groom on dressage carriages

Unlike the marathon carriage, the groom can only sit on the rear seat of a dressage carriage. Therefore, a Hanavan dummy in a typical sitting posture for dressage carriages was modelled.

For this model, the origin of coordinates was chosen to be in the sitting point and for different groom sizes, the different dummies were rotated again just like in section 3.3. In figure 3.9, the resulting posture is displayed.

The resultant data for further calculations is shown in table 3.15. Values for slight variations of the joint angles within ± 5 deg are shown in table 3.16.

The variation of the centre of gravity of the p50-driver stays within a distance of around 1.9 cm. The difference of the moment of inertia I_{zz} is about $0.3410 \text{ kg}\cdot\text{m}^2$ and the difference of the product of inertia I_{xz} and I_{yz} stays within $0.4960 \text{ kg}\cdot\text{m}^2$.

Table 3.15: Moment and product of inertia as well as the centre of gravity of the groom on dressage carriage.

| | Components of inertia tensor $[I] = \text{kg}\cdot\text{m}^2$ | | | Centre of gravity $[\vec{r}_{CG}] = \text{m}$ | | |
|-----|--|----------|----------|--|----------|----------|
| | I_{xz} | I_{yz} | I_{zz} | x_{CG} | y_{CG} | z_{CG} |
| p25 | 1.5316 | 0.0024 | 3.0385 | 0.1169 | -0.0000 | 0.1898 |
| p50 | 1.8408 | 0.0028 | 3.6396 | 0.1217 | 0.0000 | 0.2018 |
| p75 | 2.2076 | 0.0034 | 4.3655 | 0.1260 | 0.0000 | 0.2117 |

Table 3.16: Ranges for the values of moment and product of inertia as well as position of the centre of gravity of the groom on dressage carriage.

| | Components of inertia tensor $[I] = \text{kg}\cdot\text{m}^2$ | | | Centre of gravity $[\vec{r}_{CG}] = \text{m}$ | | |
|--------------------|--|----------|----------|--|----------|----------|
| | I_{xz} | I_{yz} | I_{zz} | x_{CG} | y_{CG} | z_{CG} |
| p25 _{min} | 1.3714 | -0.3647 | 3.0951 | 0.1115 | -0.0093 | 0.1865 |
| p25 _{max} | 1.5763 | 0.3503 | 3.1274 | 0.1155 | 0.0123 | 0.1905 |
| p50 _{min} | 1.6957 | -0.3557 | 3.9806 | 0.1225 | -0.0046 | 0.2033 |
| p50 _{max} | 1.9108 | 0.4988 | 3.6896 | 0.1207 | 0.0149 | 0.2037 |
| p75 _{min} | 2.0066 | -0.3078 | 4.3502 | 0.1238 | -0.0183 | 0.2079 |
| p75 _{max} | 2.1707 | 0.4650 | 4.2894 | 0.1265 | 0.0154 | 0.2114 |

Chapter 4

Dynamic system

In this chapter, the dynamic modelling of the carriage in curves with driver and groom is described. The applied model considers the entire carriage, wheels, driver and groom to be rigid bodies without any movement relative to each other. Also, the wheels are considered to be ideally rolling without any friction, any effects due to the skew or the camber angle of the wheels are not considered in the current model.

Since the model is only used to compare the influence of certain postures on the maximum velocity, no analysis of the influence of a moving groom and a change of posture was included. Also, the system considered the floor to be a flat plane without any tilt.

4.1 Dynamic model with ball joint

A draft of the carriage model with ball joint in the front axle can be seen in figure 4.1 from the top view. Here, the driver is considered to be seated in the plane of symmetry of the carriage whereas the groom can take any position in x and y . The ball joint model was chosen because the carriage is considered to be a rigid body, any effects of the suspension are neglected, and the system has to be statically determinate.

In figure 4.2, all considered forces and the two main components of the model, which are the main carriage and the front axle, can be seen. Here, F_{NW} means the normal force assigned to the wheels with the same number, F_{NJ} is the normal force of the joint. In lateral direction S_R means the combined lateral force on the wheels of the rear axle, S_F is the combined lateral force of the wheels of the front axle. Both these forces are directed to the centre of coordinates, therefore their torque around 0 is

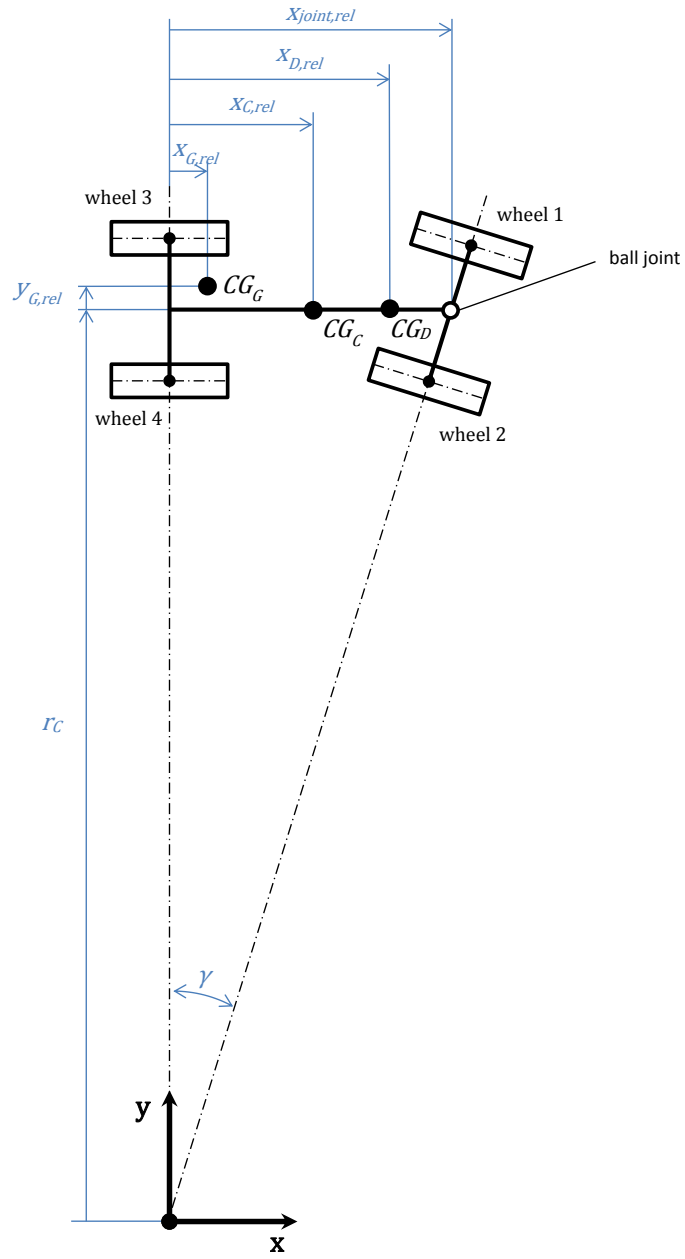


Figure 4.1: Model of carriage with ball joint in front axle.

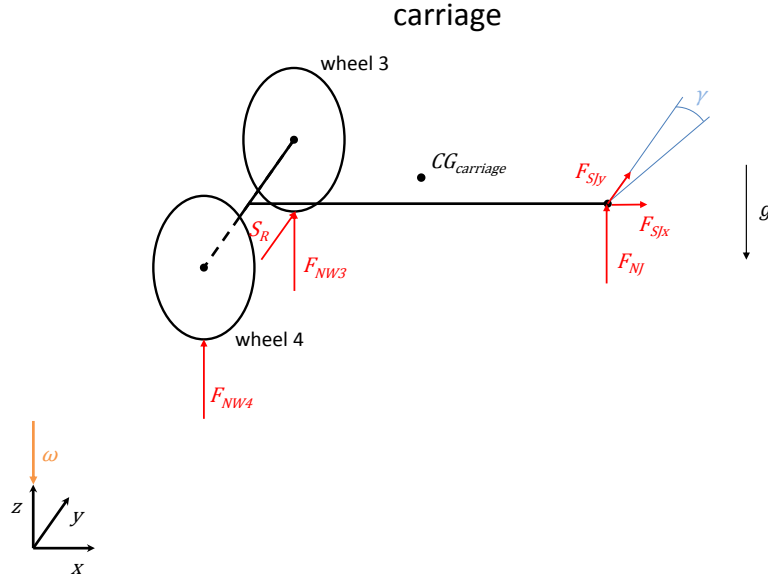


Figure 4.2: Model of the carriage and front axle including the forces.

zero. F_{SJ} is the lateral force of the ball joint. It's line of action intersects the z -axis perpendicular. Also in this draft the steering angle γ and the angular velocity $\vec{\omega}$ are shown.

For the given system the principles of angular and linear momentum have to be applied. For the purpose of collecting the elements as a sum, the elements of the carriage (*wheel 3*, *wheel 4*, *carriage*, *driver*, *groom*) are marked with index i . The forces are collected in a sequence $(F_{NW3}, F_{NW4}, F_{NJ}, S_R, F_{SJx}, F_{SJy})$ with index j for its elements.

Now, the equations for the linear momentum at constant velocity are

$$\sum m_i \begin{pmatrix} -r_{yi} \\ -r_{xi} \\ 0 \end{pmatrix} \omega_0^2 = \sum \vec{F}_j + \underbrace{\sum \vec{F}_{gi}}_{\text{forces of gravity}}, \quad (4.1)$$

and for the angular momentum they are

$$\underbrace{\sum (\vec{e}_z \times (\underbrace{\vec{I}_i \vec{e}_i}_{\frac{\vec{L}_{CGi}}{\omega_0}} + m_i (\vec{r}_i \times (\vec{e}_z \times \vec{r}_i)))) \cdot \omega_0^2}_{\frac{\vec{L}_{0i}}{\omega_0}} = \sum \vec{r}_j \times \vec{F}_j + \underbrace{\sum \vec{r}_i \times \vec{F}_{gi}}_{\text{gravitational torque}} \quad (4.2)$$

or short

$$\sum \left(\vec{e}_z \times \frac{\vec{L}_{0i}}{\omega_0} \right) \cdot \omega_0^2 = \sum \vec{M}_j + \sum \vec{M}_{gi} . \quad (4.3)$$

In equation 4.2 \vec{e}_i is a dimensionless vector pointing in the direction of the angular velocity of the component. It is scaled such, that when multiplied by ω_0 the resultant vector becomes the actual vector of the angular velocity of that component. For the carriage, driver and groom, \vec{e}_i is the unit vector in z \vec{e}_z . For a wheel i it is

$$\vec{e}_{Wi} = \begin{pmatrix} -\frac{r_{Wxi}}{r_{Wzi}} \\ -\frac{r_{Wyi}}{r_{Wzi}} \\ 1 \end{pmatrix} . \quad (4.4)$$

In the same way the, the system of equations to describe the front axle can be written. Since the front axle is actually a planar problem, only three skalar equations are needed for solving.

With the two systems of equations given in equation 4.1 and 4.2, any kind of driving analysis can be done for steady state cornering. This can be either solving for maximum velocity depending on groom positions or solving for the forces of the wheels at a given velocity.

When applying this model, it is important to keep in mind that any stabilizing effects of the suspension of the front axle are neglected. In order to compensate for that, a different point than the centre of the axle can be chosen as the location of the ball joint. This will be demonstrated in section 5.3.5

4.2 Location of the ball joint

The ball joint model allows the carriage to tip over three different axes, as can be seen in figure 4.3. Using a point mass model, to describe the cornering of the carriage, it is stable, as long as the resulting gravitational and inertial force passes through the triangle created by the three tipping line edges.

Usually when driving, the carriage will tip over the outer tipping line. The normal force on the inner wheel gets zero. In certain sharp turn manoeuvres it is also possible to tip over the inner tipping edge. The rear tipping line practically never comes into play, since the groom cannot go far enough behind the rear axle to cause tipping over the rear wheels. Therefore the criteria for tipping to the rear was simplified to be $F_{NJ} = 0$, even though, in reality the weight of the wheels would delay the rolling over.

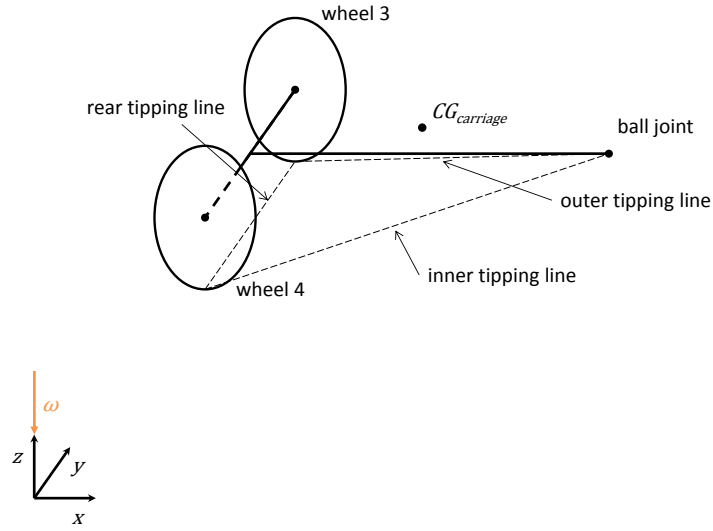


Figure 4.3: Draft of the three tipping lines of the ball joint model.

Any stabilizing or destabilizing influence of the horses' behaviour cannot be described with this model. To describe possible other modes of rolling over, the location of the ball joint can be changed. For the main simulations the location was chosen to be in the centre of the front axle. Simulations for a ball-joint at the centre of the outer front wheel or at the contact point of the outer front wheel with the ground are also possible. This cases may be a more realistic model for a turntable just allowing rotations around a vertical axis.

For initial simulations a model with ball joint at the centre of the rear axle was considered as well. But these simulations resulted in the carriage to tip over at too low velocities. Therefore, those results were discarded.

Chapter 5

Simulation results

In this chapter, the results obtained from the model with different driver and groom postures are shown. Other special analysis for sharp cornering and the influence of acceleration of the carriage on the maximum velocity are performed as well.

All the results for the maximum velocity presented in this chapter refer to the rear axle centre's velocity.

5.1 Marathon carriage

For all results of marathon carriages that follow, the positioning of the driver was adjusted the same way. The p25-driver was positioned 0.054 m further in x than the p75 driver. The p50-driver was positioned 0.024 m further in x than the p75-driver. This precaution was made because the driver's seat in marathon carriages can usually be shifted for better sitting.

5.1.1 Marathon carriage with standing groom

In table 5.1 the chosen coordinates for the position of the reference-point of the groom relative to the coordinate system of the carriage can be obtained. The values indicate that the groom stands somewhere on the rear platform between the left and right hand side of the carriage and therefore more or less close to the centre of curvature. Also the groom can change the position to get more or less close to the rear axle.

Table 5.2 shows the maximum velocities of the carriage for all combinations of driver

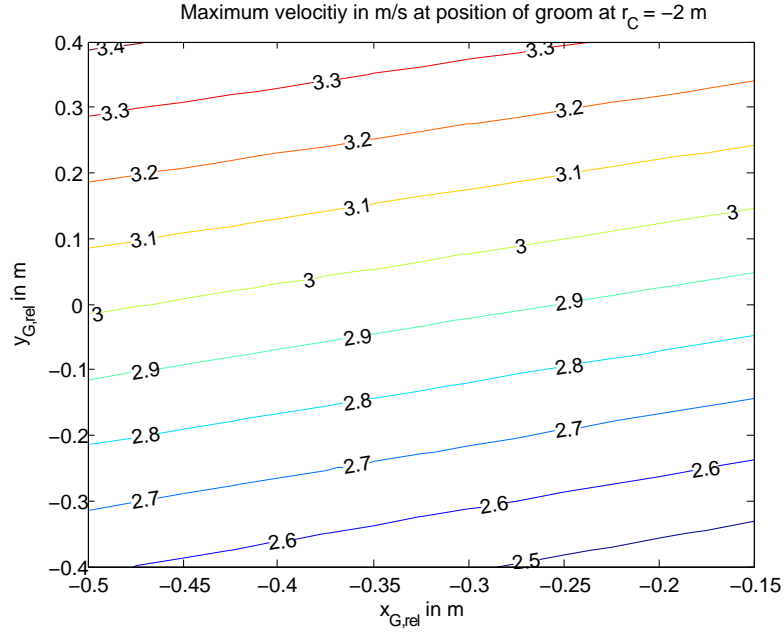


Figure 5.1: Lines of constant velocity dependent on the relative position of the standing groom.

and groom percentiles. The shown values are valid for a groom standing in the four corner positions given in table 5.1. The position of the driver remained the same, aside from the adjustment in $x_{D,rel}$ as described above. In figure 5.1, the maximum velocity of the carriage at tipping point with a p50-driver and a p50-groom for a curve radius of -2 m is shown. Negative values for the radius mean that a left turn was analysed.

Figures 5.2 and 5.3 show the maximum velocity an the four corner-positions of the groom given in table 5.1.

Table 5.1: Location range of the reference point of the standing groom.

| | | | |
|-------------|-------------------|---------|-------------------|
| | $x_{G,1}$ | | $x_{G,n}$ |
| $x_{G,rel}$ | -0.15 m | \dots | -0.50 m |
| | $y_{G,out}$ | | $y_{G,in}$ |
| $y_{G,rel}$ | -0.40 m | \dots | 0.40 m |

$$z_{G,rel} = 0.30 \text{ m}$$

Table 5.2: Maximum velocity (in m/s) for different driver and standing groom combinations at the four corner-positions and in the plane of symmetry and $r_C = -2 \text{ m}$.

| | | Driver | | | | | | |
|-------|-----|-------------|-----------|-----------|-----------|-----------|-----------|--------|
| | | p25 | | p50 | | p75 | | |
| | | $x_{G,1}$ | $x_{G,n}$ | $x_{G,1}$ | $x_{G,n}$ | $x_{G,1}$ | $x_{G,n}$ | |
| Groom | p25 | $y_{G,out}$ | 2.4561 | 2.6354 | 2.4478 | 2.6225 | 2.4377 | 2.6077 |
| | | $y_G = 0$ | 2.8668 | 3.0270 | 2.8470 | 3.0034 | 2.8250 | 2.9775 |
| | | $y_{G,in}$ | 3.2670 | 3.4131 | 3.2356 | 3.3785 | 3.2019 | 3.3414 |
| | p50 | $y_{G,out}$ | 2.4337 | 2.6244 | 2.4263 | 2.6122 | 2.4171 | 2.5981 |
| | | $y_G = 0$ | 2.8688 | 3.0384 | 2.8496 | 3.0152 | 2.8282 | 2.9899 |
| | | $y_{G,in}$ | 3.2930 | 3.4473 | 3.2618 | 3.4128 | 3.2282 | 3.3758 |
| | p75 | $y_{G,out}$ | 2.4105 | 2.6131 | 2.4040 | 2.6016 | 2.3957 | 2.5883 |
| | | $y_G = 0$ | 2.8711 | 3.0504 | 2.8524 | 3.0277 | 2.8316 | 3.0029 |
| | | $y_{G,in}$ | 3.3203 | 3.4832 | 3.2893 | 3.4488 | 3.2560 | 3.4120 |

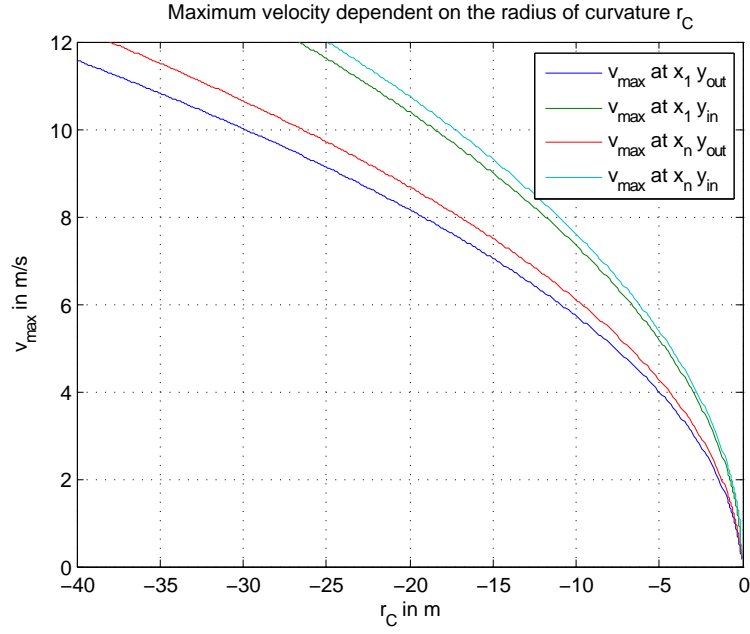


Figure 5.2: Maximum velocity for the standing groom dependent on the radius of curvature of the turn for combinations of $x_{G,1} = -0.15$ m, and $x_{G,n} = -0.50$ m with $y_{G,out} = -0.40$ m, and $y_{G,in} = 0.40$ m.

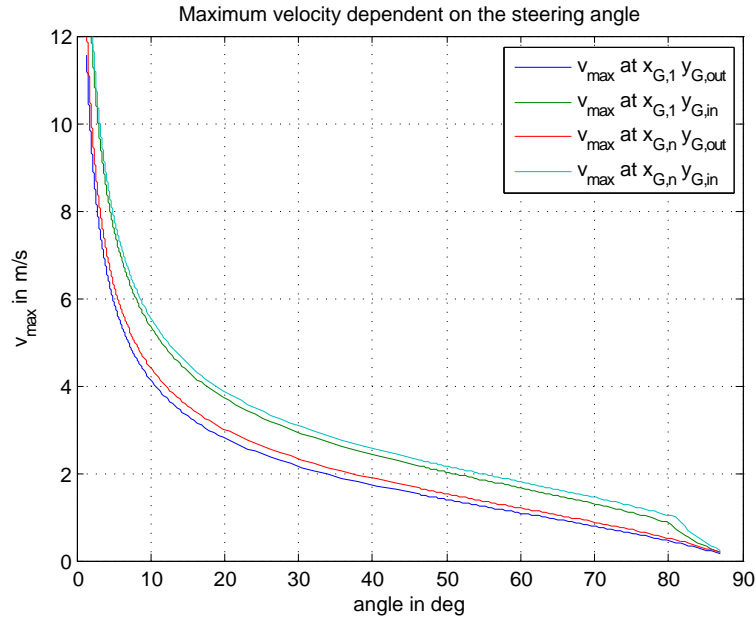


Figure 5.3: Maximum velocity for the standing groom dependent on the steering angle for combinations of $x_{G,1} = -0.15$ m, and $x_{G,n} = -0.50$ m with $y_{G,out} = -0.40$ m, and $y_{G,in} = 0.40$ m.

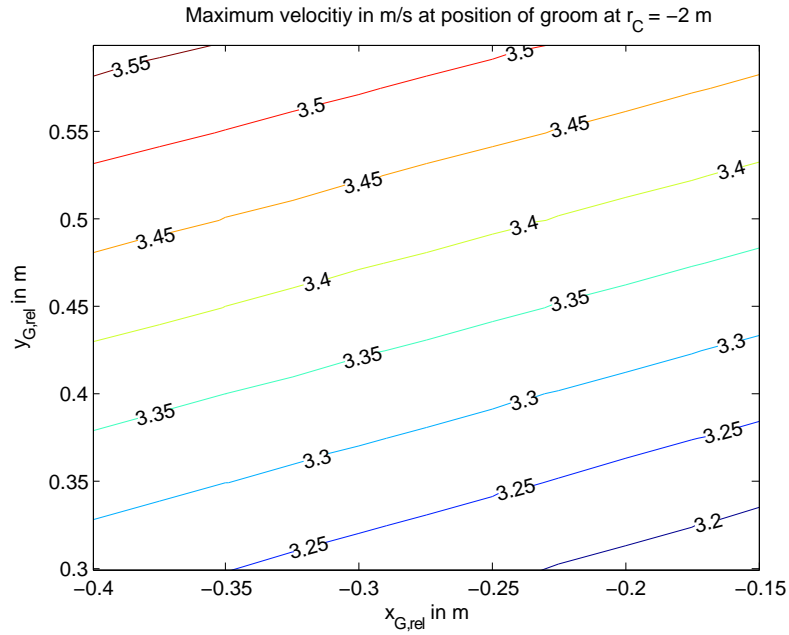


Figure 5.4: Lines of constant velocity dependent on the relative position of the straight sitting groom.

5.1.2 Marathon carriage with sitting groom

Here, the results for the sitting groom are formatted the same way as in section 5.1.1.

In figures 5.4 through 5.6, the results are shown for a straight sitting p50-groom and a p50-driver. As seen in table 5.4, the results for different kinds of sitting posture vary only a little.

Table 5.3: Location range of the reference point of the sitting groom.

| | | | |
|------------------------------|-------------------|---------|-------------------|
| | $x_{G,1}$ | | $x_{G,n}$ |
| $x_{G,rel}$ | -0.15 m | \dots | -0.40 m |
| | $y_{G,1}$ | | $y_{G,n}$ |
| $y_{G,rel}$ | 0.30 m | \dots | 0.60 m |
| $z_{G,rel} = 0.88 \text{ m}$ | | | |

Table 5.4: Maximum velocity (in m/s) for different driver and sitting groom combinations at the four corner-positions at $r_C = -2 \text{ m}$.

| | | | Driver | | | | | |
|--|-----|-----------|-----------|-----------|-----------|-----------|-----------|-----------|
| | | | p25 | | p50 | | p75 | |
| | | | $x_{G,1}$ | $x_{G,n}$ | $x_{G,1}$ | $x_{G,n}$ | $x_{G,1}$ | $x_{G,n}$ |
| Groom sitting straight | p25 | $y_{G,1}$ | 3.1698 | 3.2742 | 3.1406 | 3.2428 | 3.1092 | 3.2090 |
| | | $y_{G,n}$ | 3.4644 | 3.5610 | 3.4265 | 3.5211 | 3.3861 | 3.4787 |
| | p50 | $y_{G,1}$ | 3.1931 | 3.3033 | 3.1641 | 3.2719 | 3.1327 | 3.2381 |
| | | $y_{G,n}$ | 3.5059 | 3.6075 | 3.4677 | 3.5673 | 3.4270 | 3.5246 |
| | p75 | $y_{G,1}$ | 3.2180 | 3.3341 | 3.1891 | 3.3027 | 3.1578 | 3.2690 |
| | | $y_{G,n}$ | 3.5498 | 3.6565 | 3.5114 | 3.6161 | 3.4705 | 3.5731 |
| Groom leaning | p25 | $y_{G,1}$ | 3.2235 | 3.3264 | 3.1926 | 3.2932 | 3.1593 | 3.2577 |
| | | $y_{G,n}$ | 3.5182 | 3.6133 | 3.4784 | 3.5716 | 3.4361 | 3.5273 |
| | p50 | $y_{G,1}$ | 3.2510 | 3.3595 | 3.2201 | 3.3263 | 3.1869 | 3.2907 |
| | | $y_{G,n}$ | 3.5641 | 3.6640 | 3.5239 | 3.6219 | 3.4812 | 3.5772 |
| | p75 | $y_{G,1}$ | 3.2794 | 3.3936 | 3.2486 | 3.3604 | 3.2153 | 3.3248 |
| | | $y_{G,n}$ | 3.6118 | 3.7166 | 3.5713 | 3.6742 | 3.5283 | 3.6291 |
| Groom sitting straight and stretching leg | p25 | $y_{G,1}$ | 3.1602 | 3.2650 | 3.1314 | 3.2339 | 3.1003 | 3.2004 |
| | | $y_{G,n}$ | 3.4549 | 3.5519 | 3.4173 | 3.5123 | 3.3773 | 3.4702 |
| | p50 | $y_{G,1}$ | 3.1826 | 3.2932 | 3.1539 | 3.2621 | 3.1229 | 3.2286 |
| | | $y_{G,n}$ | 3.4955 | 3.5975 | 3.4576 | 3.5576 | 3.4173 | 3.5152 |
| | p75 | $y_{G,1}$ | 3.2064 | 3.3229 | 3.1779 | 3.2919 | 3.1470 | 3.2586 |
| | | $y_{G,n}$ | 3.5383 | 3.6454 | 3.5003 | 3.6054 | 3.4597 | 3.5627 |
| Groom leaning and stretching leg | p25 | $y_{G,1}$ | 3.2138 | 3.3171 | 3.1833 | 3.2842 | 3.1503 | 3.2490 |
| | | $y_{G,n}$ | 3.5087 | 3.6041 | 3.4692 | 3.5627 | 3.4272 | 3.5188 |
| | p50 | $y_{G,1}$ | 3.2404 | 3.3492 | 3.2099 | 3.3164 | 3.1769 | 3.2811 |
| | | $y_{G,n}$ | 3.5535 | 3.6538 | 3.5137 | 3.6121 | 3.4714 | 3.5677 |
| | p75 | $y_{G,1}$ | 3.2677 | 3.3823 | 3.2372 | 3.3495 | 3.2044 | 3.3142 |
| | | $y_{G,n}$ | 3.6001 | 3.7054 | 3.5600 | 3.6633 | 3.5174 | 3.6186 |

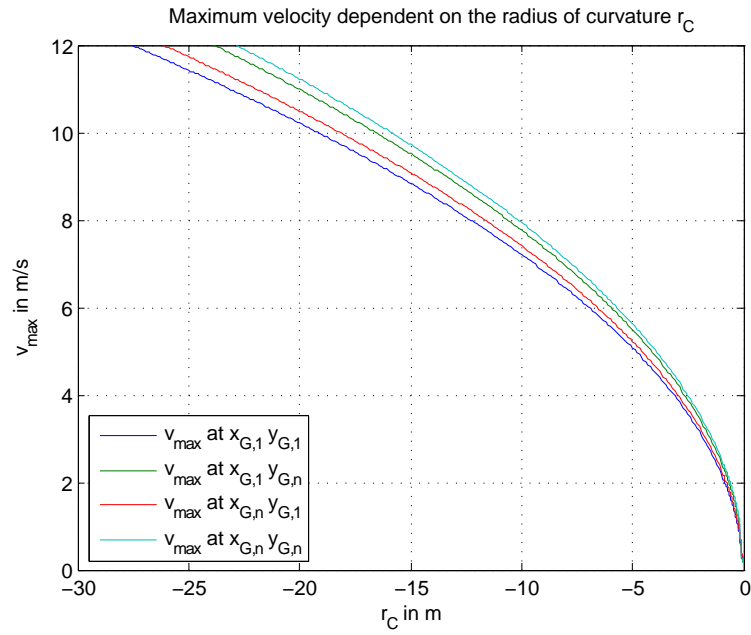


Figure 5.5: Maximum velocity for the straight sitting groom dependent on the radius of curvature of the turn for combinations of $x_{G,1} = -0.15$ m, and $x_{G,n} = -0.40$ m with $y_{G,1} = 0.30$ m, and $y_{G,n} = 0.60$ m.

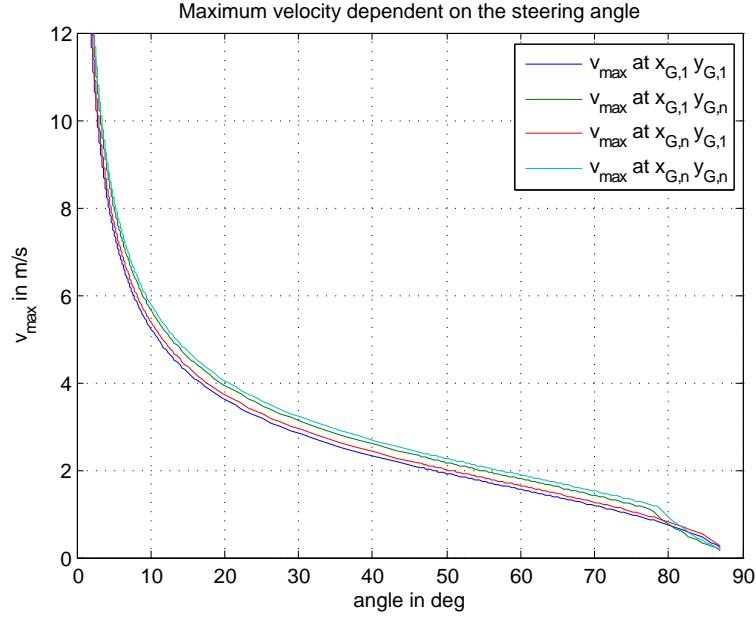


Figure 5.6: Maximum velocity for the straight sitting groom dependent on the steering angle for combinations of $x_{G,1} = -0.15$ m, and $x_{G,n} = -0.40$ m with $y_{G,1} = 0.30$ m, and $y_{G,n} = 0.60$ m.

5.1.3 Marathon carriage with crouching groom

The following results are again formatted as in section 5.1.1. Again, only the position of the crouching groom is different, the chosen values can be obtained in table 5.5.

In figure 5.7 to 5.9, the results are shown for a crouching p50-groom and a p50-driver.

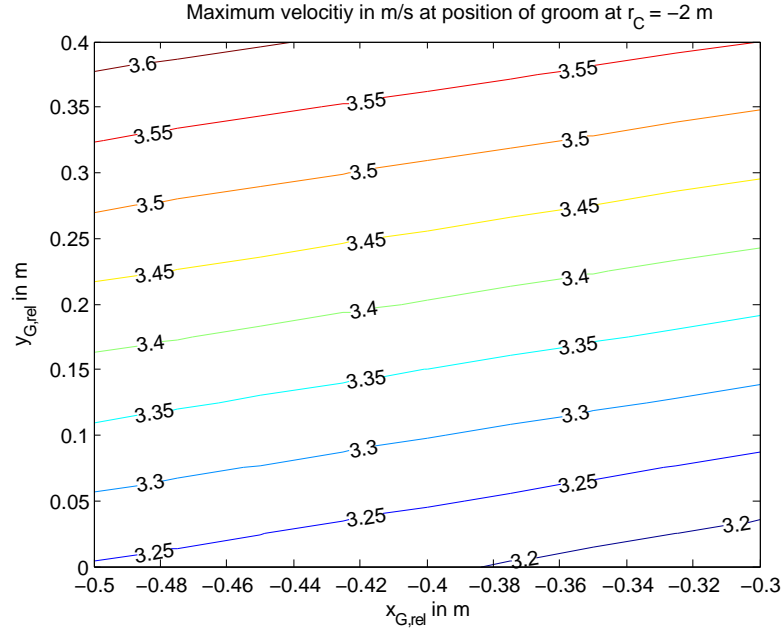


Figure 5.7: Lines of constant velocity dependent on the relative position of the crouching groom.

Table 5.5: Location range of the reference point of the crouching groom.

| | | | |
|----------------------|-----------|-----|-----------|
| | $x_{G,1}$ | | $x_{G,n}$ |
| $x_{G,rel}$ | -0.30 m | ... | -0.50 m |
| | $y_{G,1}$ | | $y_{G,n}$ |
| $y_{G,rel}$ | 0.00 m | ... | 0.40 m |
| $z_{G,rel} = 0.30$ m | | | |

Table 5.6: Maximum velocity (in m/s) for different driver and crouching groom combinations at the four corner-positions at $r_C = -2$ m.

| | | | Driver | | | | | |
|-------|-----|-----------|-----------|-----------|-----------|-----------|-----------|-----------|
| | | | p25 | | p50 | | p75 | |
| | | | $x_{G,1}$ | $x_{G,n}$ | $x_{G,1}$ | $x_{G,n}$ | $x_{G,1}$ | $x_{G,n}$ |
| Groom | p25 | $y_{G,1}$ | 3.1683 | 3.2468 | 3.1392 | 3.2161 | 3.1078 | 3.1830 |
| | | $y_{G,n}$ | 3.5409 | 3.6101 | 3.5010 | 3.5690 | 3.4586 | 3.5253 |
| | p50 | $y_{G,1}$ | 3.1947 | 3.2774 | 3.1657 | 3.2467 | 3.1343 | 3.2136 |
| | | $y_{G,n}$ | 3.5898 | 3.6623 | 3.5495 | 3.6208 | 3.5067 | 3.5767 |
| | p75 | $y_{G,1}$ | 3.2229 | 3.3098 | 3.1939 | 3.2791 | 3.1626 | 3.2461 |
| | | $y_{G,n}$ | 3.6416 | 3.7174 | 3.6010 | 3.6755 | 3.5578 | 3.6311 |

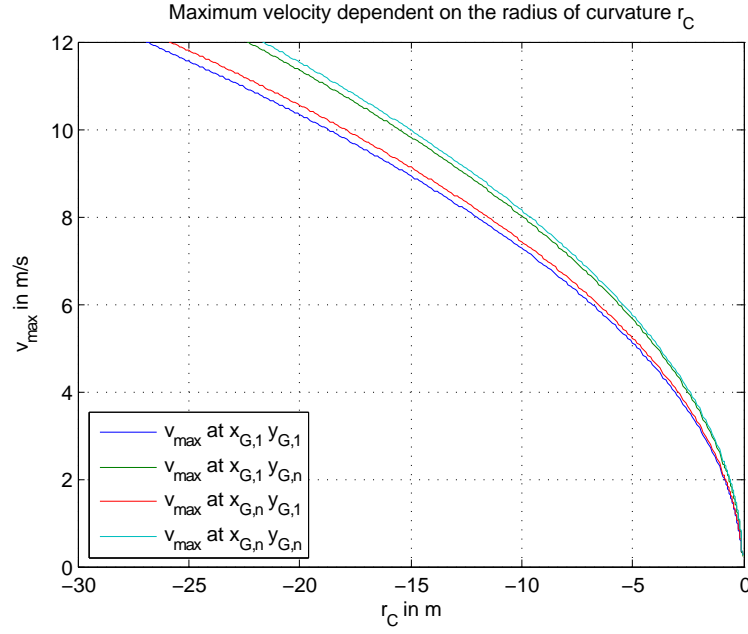


Figure 5.8: Maximum velocity for the crouching groom dependent on the radius of curvature of the turn for combinations of $x_{G,1} = -0.30$ m, and $x_{G,n} = -0.50$ m with $y_{G,1} = 0$ m, and $y_{G,n} = 0.40$ m.

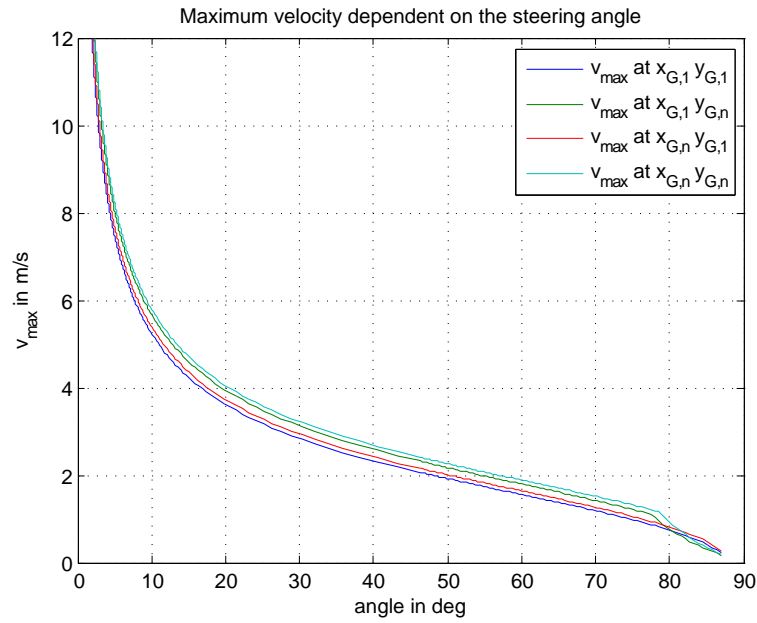


Figure 5.9: Maximum velocity for the crouching groom dependent on the steering angle for combinations of $x_{G,1} = -0.30$ m, and $x_{G,n} = -0.50$ m with $y_{G,1} = 0$ m, and $y_{G,n} = 0.40$ m.

5.1.4 Comparison of the postures

Comparing the results from tables 5.2, 5.4 and 5.6, it turns out that the recommended posture is crouching. Although leaning groom without stretched leg can achieve approximately the same velocity, but this posture is considered to increase the risk of falling of. Additionally it is harder for the leaning groom to switch posture than for the crouching groom. For a p50-driver and groom, the difference in speed of a crouching and standing groom in the best corner-position is 0.2080 m/s (which is 5.7% of the maximum velocity), whereas the difference between crouching on the inner side of the curve and the middle of the carriage is 0.3741 m/s (which is about 10.3%). Both moving to the inner side of the curve as well as lowering the centre of gravity have a positive influence on the maximum velocity. Another advantageous aspect of the crouching posture is that while the feet keep the same position, the centre of gravity does not only move downwards but, also further to the back.

The best combination of driver and groom is always the one with the lightest possible driver and the heaviest groom. This again is mostly due to the influence on the height of the centre of gravity of the entire system. However, any disadvantages a heavy groom might bring to acceleration and braking are not considered in this analysis.

In table 5.4, the maximum velocity of the sitting postures for each of the corner-positions is listed. Here, the straight sitting posture with stretched leg turns out to allow the lowest velocity, whereas the posture leaning without stretched leg allows the highest. But the difference between these two postures i.e. for the p50- driver and groom is only 0.0643 m/s or 1.8% because the position of the grooms centre of gravity is varies only very little from sitting posture to sitting posture. On the other hand, the sitting postures provide an advantage over the standing posture, since the grooms centre of gravity is lower and can be moved further to the inner side of the curve.

5.2 Dressage carriage

Unlike section 5.1, the seat of a dressage carriage usually cannot be adjusted, therefore the position of the driver is kept the same for the different percentiles.

Also, the groom can only sit in one position and must not move. Despite that fact, the influence of sitting on the inside or outside with respect to the turn is shown in figures 5.10 to 5.12. In table 5.8, the maximum velocities for each driver and groom combination sitting on the inside of the curve, the outside of the curve or in the symmetry plane are shown. The position of the groom in x is -0.22 m and in z it is

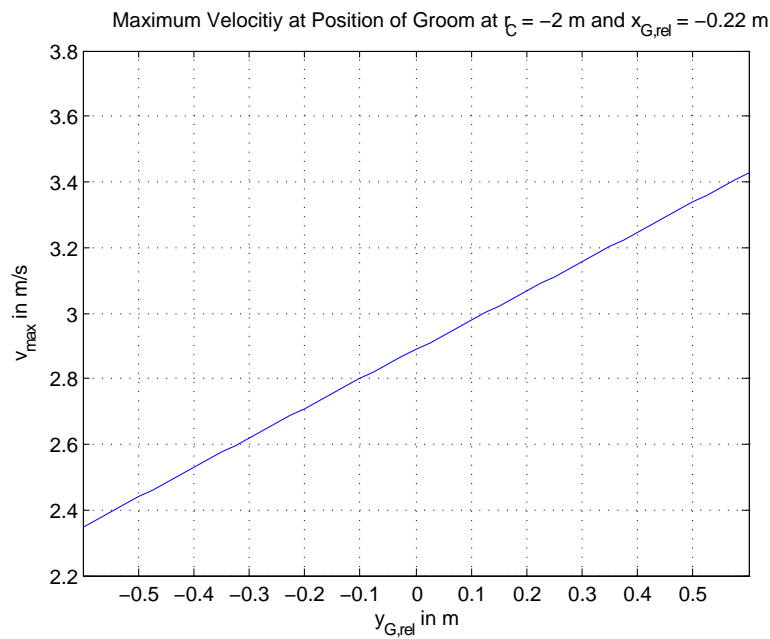


Figure 5.10: Maximum velocity dependent on the relative position of the sitting groom.

1.34 m. Only the y values are varied.

Here again, sitting as far as possible on the inner side of the curve, as well as combining a light driver with a heavy groom allows the highest velocities.

Table 5.7: Location range of the reference point of the groom on dressage carriage.

$$x_{G,rel} = -0.22 \text{ m}$$

| | | | |
|-------------|-------------------|---------|------------------|
| | $y_{G,out}$ | | $y_{G,in}$ |
| $y_{G,rel}$ | -0.60 m | \dots | 0.60 m |

$$z_{G,rel} = 1.34 \text{ m}$$

Table 5.8: Maximum velocity (in m/s) for different driver and groom combinations on a dressage carriage at $r_C = -2 \text{ m}$.

| | | | Driver | | |
|-------|-----|-------------|--------|--------|--------|
| | | | p25 | p50 | p75 |
| Groom | p25 | $y_{G,out}$ | 2.4151 | 2.3900 | 2.3640 |
| | | $y_G = 0$ | 2.9353 | 2.8987 | 2.8606 |
| | | $y_{G,in}$ | 3.4553 | 3.4054 | 3.3538 |
| | p50 | $y_{G,out}$ | 2.3816 | 2.3578 | 2.3333 |
| | | $y_G = 0$ | 2.9339 | 2.8983 | 2.8612 |
| | | $y_{G,in}$ | 3.4864 | 3.4371 | 3.3858 |
| | p75 | $y_{G,out}$ | 2.3468 | 2.3245 | 2.3013 |
| | | $y_G = 0$ | 2.9330 | 2.8984 | 2.8625 |
| | | $y_{G,in}$ | 3.5198 | 3.4710 | 3.4202 |

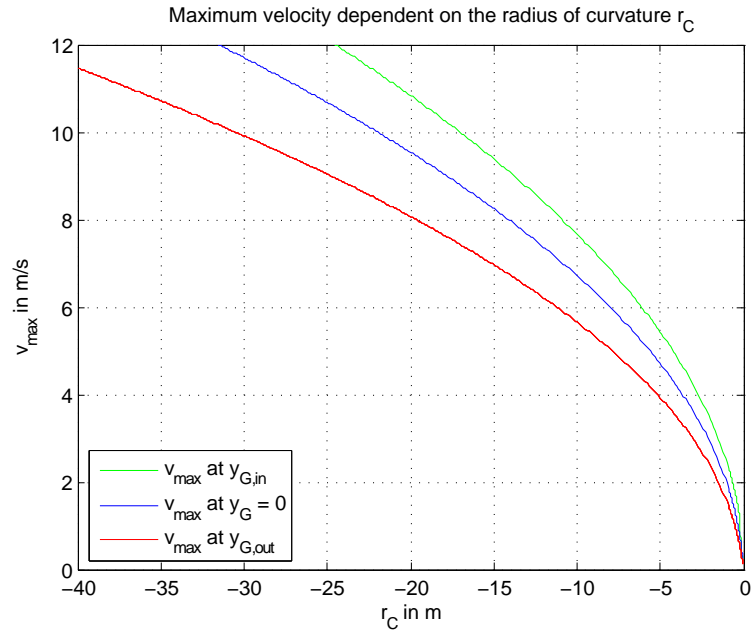


Figure 5.11: Maximum velocity for the groom dependent on the radius of curvature of the turn for $x_{G,rel} = -0.22$ m with $y_{G,in} = 0.60$ m, and $y_{G,out} = -0.60$ m.

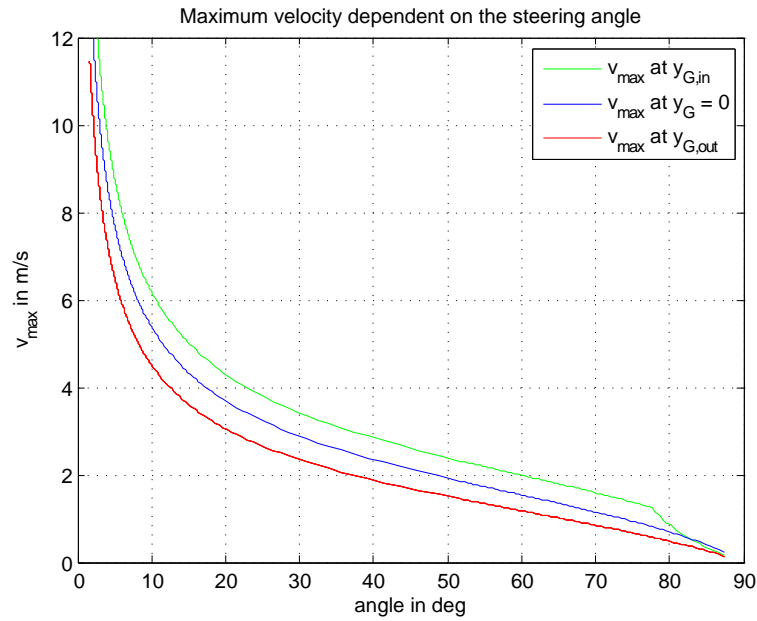


Figure 5.12: Maximum velocity for the groom dependent steering angle for $x_{G,rel} = -0.22$ m with $y_{G,in} = 0.60$ m, and $y_{G,out} = -0.60$ m.

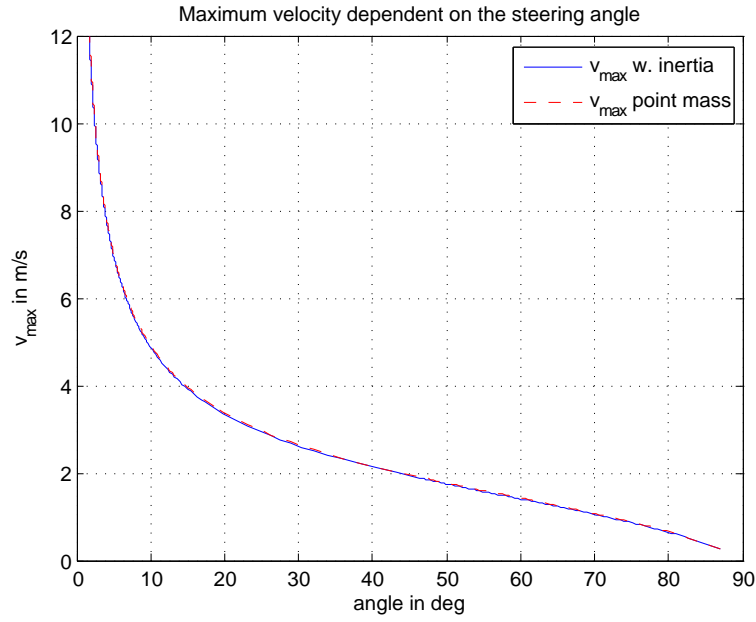


Figure 5.13: Maximum velocity of point mass model and model with inertia-tensor.

5.3 Additional simulations

In this section, certain special cases of model variation or certain characteristics of the system are discussed.

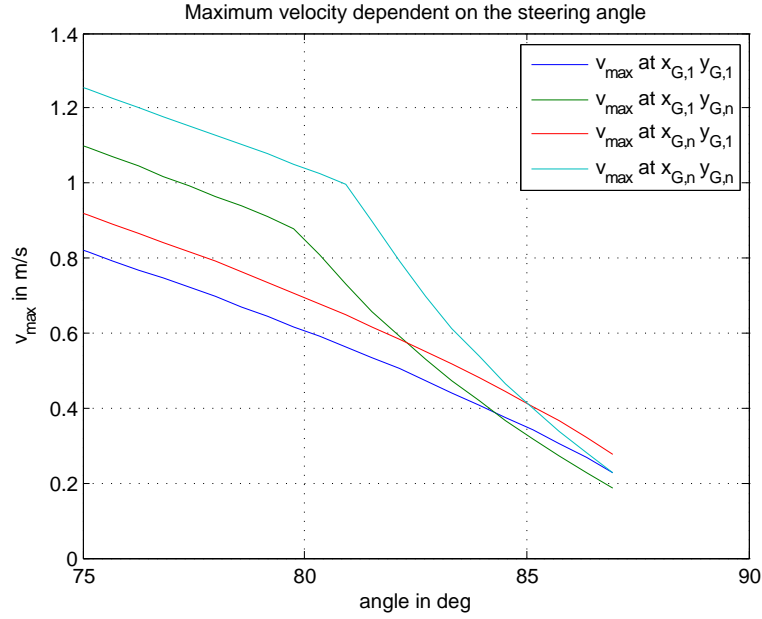
5.3.1 Influence of the inertia-tensor of the carriage and humans

The influence of the inertia-tensors of the carriage components as well as driver and groom on the maximum velocity are now looked at more closely. The results for the maximum velocities for a marathon carriage with a p50-driver and groom, positioned in the carriage's plane of symmetry at $x_{G,rel} = -0.3$ m are displayed in figure 5.13.

The inertia-tensors barely influence the maximum velocity of this rigid model of carriage. In table 5.9 various maximum velocities for different kinds of models and their regarded inertia-tensors are displayed. It can be seen that the inertia-tensor causes the carriage to tip over at lower velocities, and most of that is caused by the inertia-tensor of the wheels.

Table 5.9: Maximum velocity for -2 m curves with or without inertia-tensor.

| | v_{max} |
|---|------------|
| model with inertia-tensor: | 2.9221 m/s |
| model without inertia-tensor: | 2.9511 m/s |
| model without inertia-tensor on wheels: | 2.9451 m/s |
| model with inertia-tensor only on wheels: | 2.9279 m/s |

Figure 5.14: Maximum velocity dependent on the steering angle for combinations of $x_{G,1} = -0.15$ m, and $x_{G,n} = -0.50$ m with $y_{G,1} = 0$ m, and $y_{G,n} = 0.40$ m.

5.3.2 Sharp cornering

Cornering at steering angles of 80 deg or more cause the carriage to behave differently than in typical curves of 2 m or more. If the groom stands on the inner side of the curve, the carriage might roll over the inner tipping line.

In figures 5.15 to 5.14, the behaviour of the carriage in such sharp cornering manoeuvres is displayed. The results were generated using a standing p50-driver and groom with the same positioning as given in section 5.1.1.

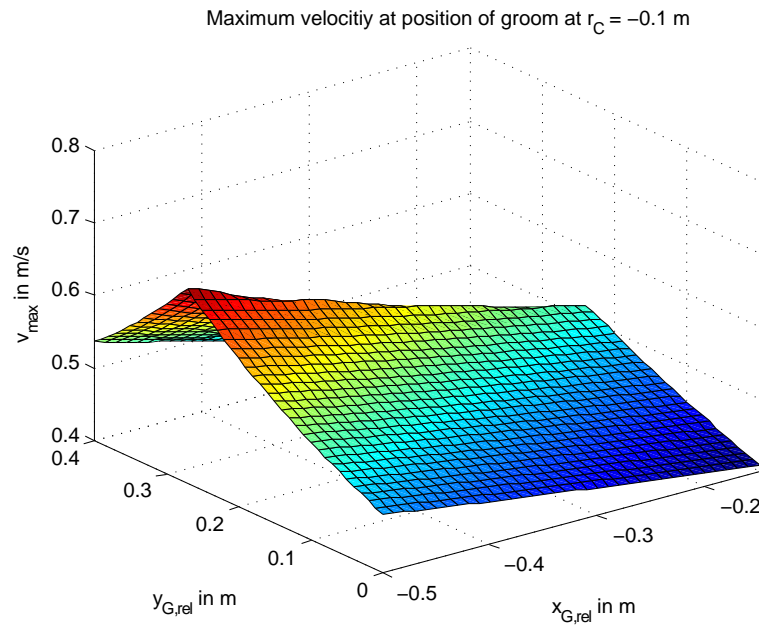


Figure 5.15: Maximum velocity dependent on the relative position of the groom.

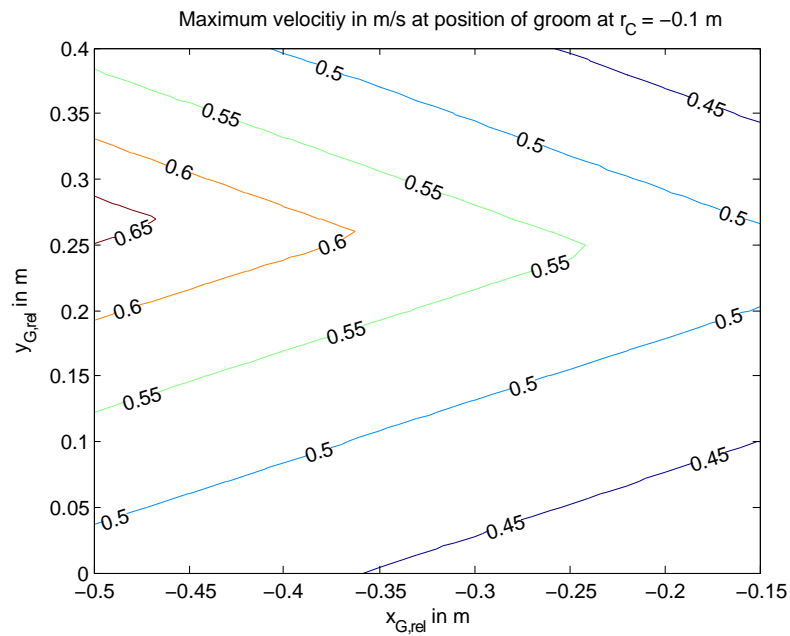


Figure 5.16: Lines of constant velocity dependent on the relative position of the groom.

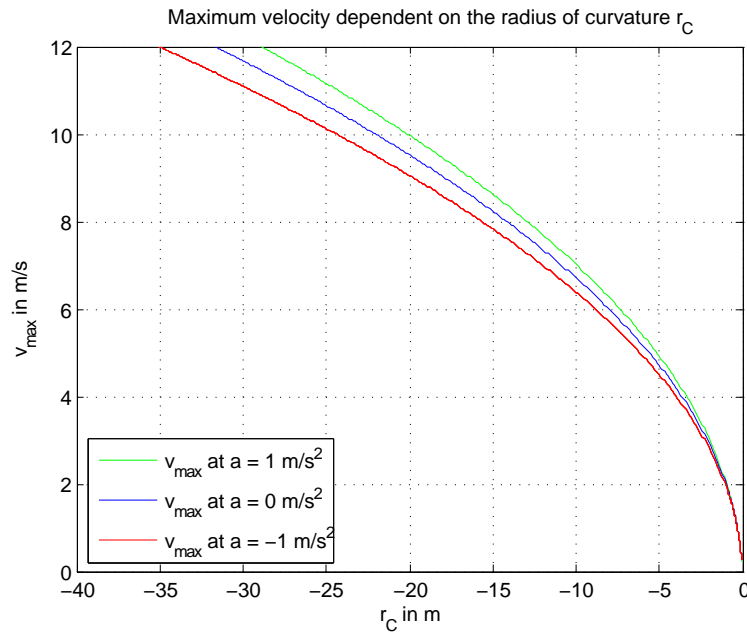


Figure 5.17: Maximum velocity dependent on the radius of curvature of the turn.

5.3.3 Influence of acceleration

In figures 5.17 and 5.18 the results for an accelerating and decelerating carriage while cornering are shown. For these figures a p50-driver and a standing p50-groom were considered and positioned the same way as in section 5.3.1.

The given acceleration of $\pm 1 \text{ m/s}^2$ is given for in the centre of the front axle, and directed tangential to the path. However, this calculation can not be considered exact, since the horses can not apply an accelerating force that is parallel to the xy-plane, as it was considered here. Also, for decelerating a carriage has its own brakes and does not solely rely on the horses. In the given example the wheels are considered to have no torque in the wheel hub.

Still, this example demonstrates that decelerating in curves causes a higher risk of rolling over for the carriage whereas accelerating has a positive effect.

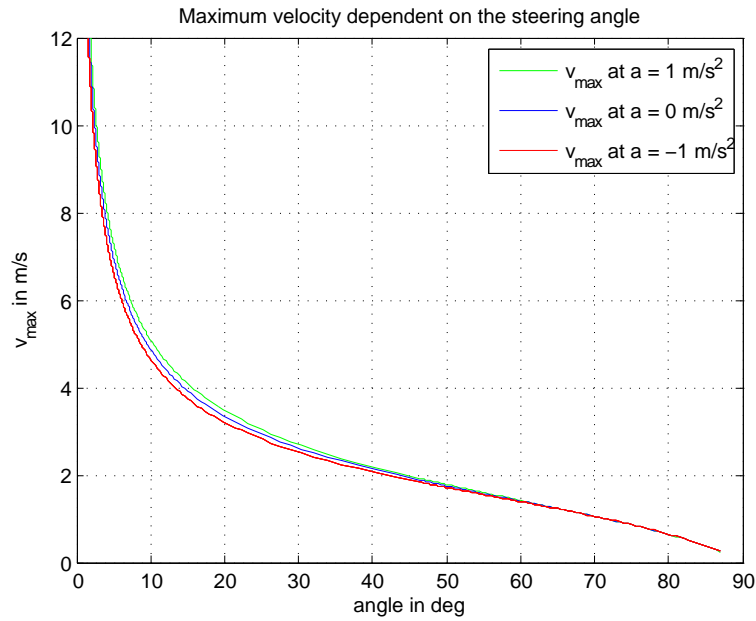


Figure 5.18: Maximum velocity dependent on the steering angle.

5.3.4 Influence of the height of the ball joint

All previous results had in common that positioning the groom further to the rear provides an advantage over positions rather close the carriage's centre of gravity. At a first view this seems to be counter-intuitive, since the height of the ball joint and therefore the three dimensional position of the tipping lines should favour a position more in the front. But this is only true above a certain height of the ball joint.

In figures 5.19 and 5.20 the optimal velocities for a carriage with ball joint between the front wheels, but with a height of 0.9724 m, which is 2.6 times the usual height of 0.3740 m, are displayed. The results were generated using a p50-driver and groom in the same positions as in section 5.1.1.

This variation of the model calculates high maxima of the velocity when compared to the result displayed in figure 5.1. When comparing figure 5.1 and 5.20 one can obtain that from a certain relative position the effect of better performance when moving forward instead of backward comes into play. This effect increases with increasing height of the ball joint until moving to the front always has a positive effect.

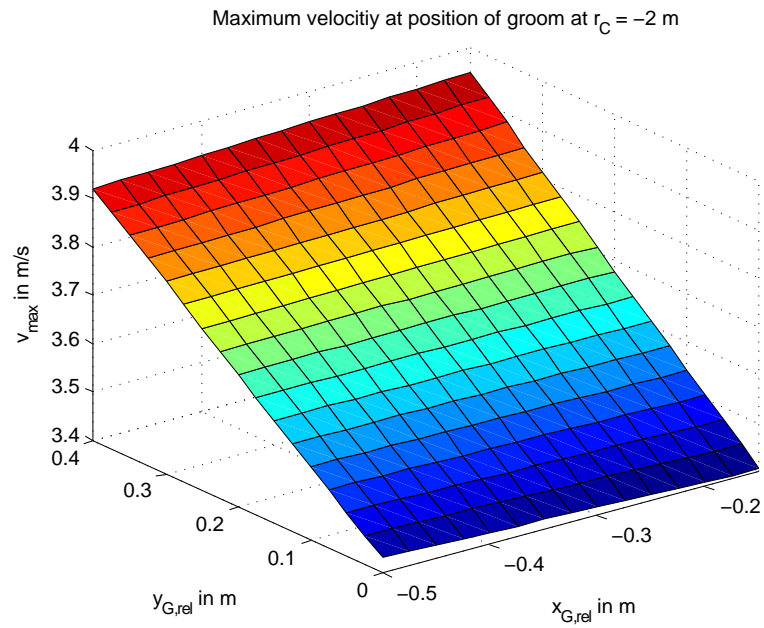


Figure 5.19: Maximum velocity dependent on the relative position of standing p50-groom.

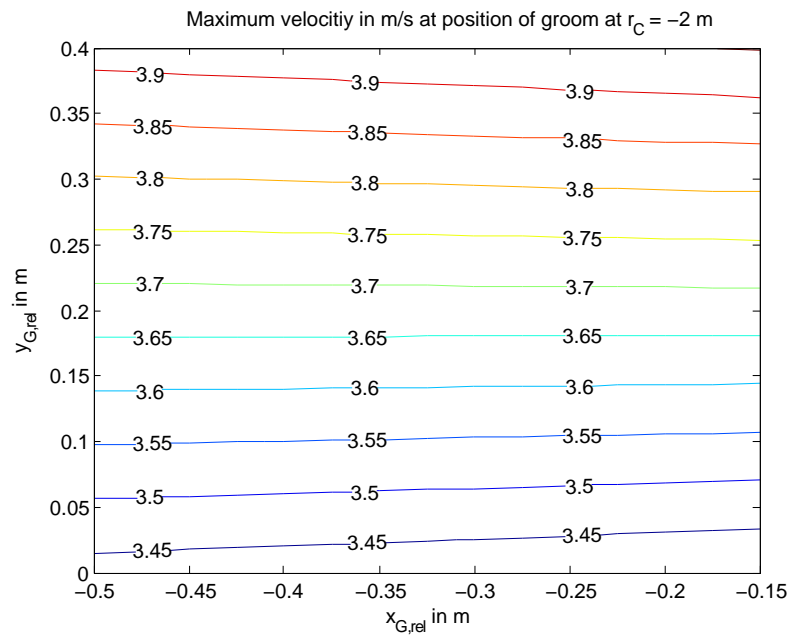


Figure 5.20: Lines of constant velocity dependent on the relative position of the p50-groom.

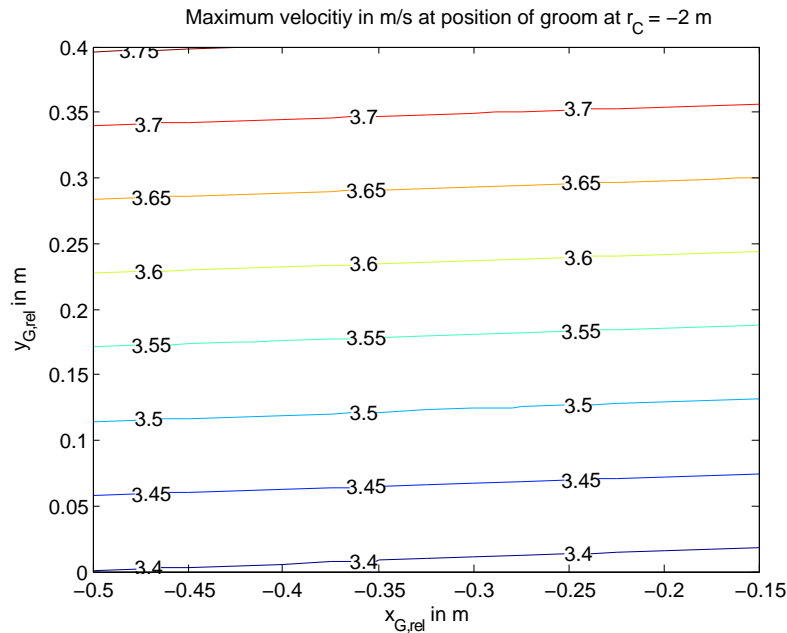


Figure 5.21: Lines of constant velocity dependent on the relative position of the p50-groom.

5.3.5 Locating the ball joint in the contact point of the outer front wheel

So far, all the given results had in common that the ball joint was located in between the front wheels. This kind of model appears to fit relatively well when applied for simulating curves with rather small radii, however, it is expected to calculate slightly too low maximum velocities with increasing radius.

For this investigation, the location of the ball joint was changed to the contact point of the outer front wheel of the carriage. The displayed results were generated using a p50-driver and standing groom with a similar positioning as in sec 5.1.1, but here, only the left half plane starting from $y = 0$ is considered.

The results in figure 5.21 allow significantly higher velocities. Also they show that moving the groom further back does have less significant influence than in section 5.1.1. The results for the gouching groom at the same location of feet is again better than the standing one with a maximum velocity of 3.9126 m/s versus 3.7537 m/s of the standing groom. The influence of the location of the groom on the x -axis might be overrated when applying the model with the ball joint in the centre of the front axle

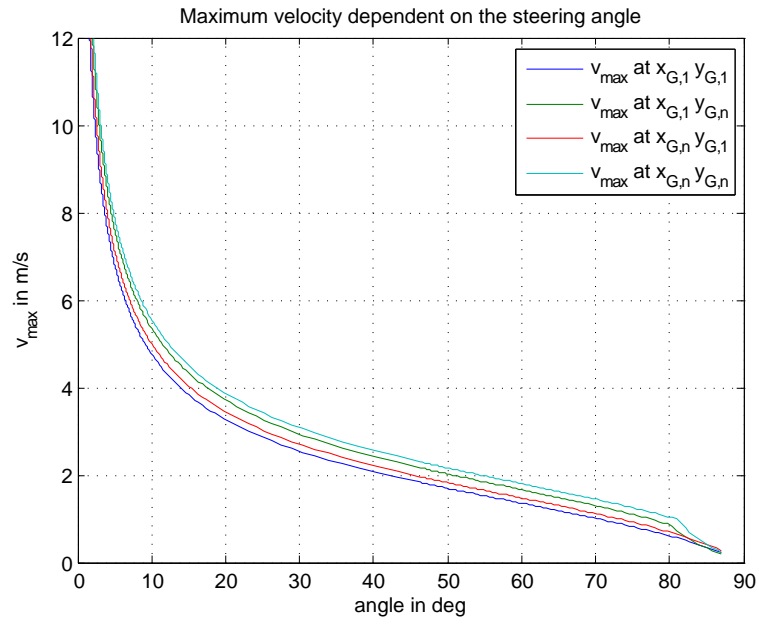


Figure 5.22: Maximum velocity dependent on the steering angle for combinations of $x_{G,1} = -0.15$ m, and $x_{G,n} = -0.50$ m with $y_{G,1} = 0$ m, and $y_{G,n} = 0.40$ m.

Chapter 6

Conclusion and outlook

In this thesis the influence of the driver and groom on the maximum velocity of carriages in curves has been investigated. Feasible models for both the carriage and the human body were found and applied in simulation.

The modelling of the inertia tensor of the carriage given in chapter 2 could not be validated with an inertia measurement. Therefore it remains unknown how well the given moments and products of inertia recreate the real behaviour. Yet regarding the influence of the parallel axis theorem given in table 2.5 and the difference of the results of the carriage with or without inertia tensor given in table 5.9, it turns out that the inertia tensor barely affects the maximum velocity. When taking the inertia tensor in consideration, the focus should lie on generating a valid model of the wheels. They have the highest impact on the results compared to all other components and human inertia tensors. Additionally, the precise measurement of the weights and calculation of the carriages centre of gravity are very important.

Concerning the modelling of the human body, the Hanavan [6] model seems to be well fitting. Just as for the carriage, the calculated inertia tensors might be disregarded, but the calculated centres of gravity for the different postures can still be applied. Also, for individual analysis, only 25 anthropometric parameters are needed. Concerning slight variations of the posture as they practically always occur while driving, an estimation of the change of the inertia tensor and the centre of gravity was done as well. Since the human bodies are always considered to be rigid and not moving, there are no predictions given how strong human movement and dynamic changes in posture can influence the behaviour of the carriage.

If another mathematical model of the human body with higher complexity has to be applied, the model after Yeadon [16] can be suggested. Also, one of the first investigations further than the ones presented here is the influence of the moving

groom. Here, especially the posture change as well as a change of position from the outer to the inner side of the curve should be analysed.

When looking at the results given in chapter 5, it can be seen that the recommended posture of the groom is to crouch in the rear of the carriage on the inner side of the turn. This also shows that the influence of moving the centre of gravity downwards versus moving it to the inner side of the curve should not be disrespected. The second best posture for the groom turned out to be sitting on the side of the carriage. Concerning the maximum velocity, these two postures are almost equal, but the leaning posture without stretched leg is rather risky compared to crouching.

While comparing the different sitting postures, it turned out that the different kinds of sitting postures only have very little impact on the behaviour of the entire carriage. While the leaning posture without stretching one leg away might provide a slight advantage, there is no actual reason to risk a safe sitting posture where the groom uses both hands and feet to hold on to the carriage.

While the model of the carriage can definitely be applied in order to find the optimal posture for the groom, it should be improved for further investigations. Comparing the velocities in figure 5.1 and figure 5.21 it turns out that the value of the maximum velocity is highly dependent on the location of the ball joint.

A first suggestion for an advanced model is to apply two linear torsion springs in the centre of the front and rear axle, instead of considering the entire carriage to be a rigid body. The main difficulty here would lie in the identification of a feasible spring constant. The inclusion of tilting of the carriage as well as adding a stabilising effect to the front axle should increase the accuracy of the model predictions significantly.

List of Figures

| | | |
|-----|--|----|
| 1.1 | A racing team on a marathon carriage. | 2 |
| 2.1 | Rod model of the turntable. | 5 |
| 2.2 | Rod and plate model of the marathon carriage. | 6 |
| 2.3 | Rod model of the dressage carriage. | 9 |
| 2.4 | Draft of the geometry for applying the trifilar pendulum method. . . | 12 |
| 3.1 | Overlap of sitting driver and positioned p75 dummy. | 15 |
| 3.2 | Posture of the p75-dummy as driver. | 16 |
| 3.3 | Posture of the p75-dummy as standing groom. | 19 |
| 3.4 | Posture of the p75-dummy as straight sitting groom. | 20 |
| 3.5 | Posture of the p75-dummy as leaning groom. | 22 |
| 3.6 | Posture of the p75-dummy as sitting groom with stretched leg. . . . | 23 |
| 3.7 | Posture of the p75-dummy as leaning groom with stretched leg. . . . | 25 |
| 3.8 | Posture of the p75-dummy as crouching groom. | 28 |
| 3.9 | Posture of the p75-dummy as groom on dressage carriage. | 29 |
| 4.1 | Model of carriage with ball joint in front axle. | 32 |
| 4.2 | Model of the carriage and front axle including the forces. | 33 |
| 4.3 | Draft of the three tipping lines of the ball joint model. | 35 |
| 5.1 | Lines of constant velocity dependent on the relative position of the standing groom. | 37 |
| 5.2 | Maximum velocity for the standing groom dependent on the radius of curvature of the turn for combinations of $x_{G,1} = -0.15$ m, and $x_{G,n} = -0.50$ m with $y_{G,out} = -0.40$ m, and $y_{G,in} = 0.40$ m. | 39 |
| 5.3 | Maximum velocity for the standing groom dependent on the steering angle for combinations of $x_{G,1} = -0.15$ m, and $x_{G,n} = -0.50$ m with $y_{G,out} = -0.40$ m, and $y_{G,in} = 0.40$ m. | 39 |
| 5.4 | Lines of constant velocity dependent on the relative position of the straight sitting groom. | 40 |
| 5.5 | Maximum velocity for the straight sitting groom dependent on the radius of curvature of the turn for combinations of $x_{G,1} = -0.15$ m, and $x_{G,n} = -0.40$ m with $y_{G,1} = 0.30$ m, and $y_{G,n} = 0.60$ m. | 42 |

| | | |
|------|--|----|
| 5.6 | Maximum velocity for the straight sitting groom dependent on the steering angle for combinations of $x_{G,1} = -0.15$ m, and $x_{G,n} = -0.40$ m with $y_{G,1} = 0.30$ m, and $y_{G,n} = 0.60$ m. | 43 |
| 5.7 | Lines of constant velocity dependent on the relative position of the crouching groom. | 44 |
| 5.8 | Maximum velocity for the crouching groom dependent on the radius of curvature of the turn for combinations of $x_{G,1} = -0.30$ m, and $x_{G,n} = -0.50$ m with $y_{G,1} = 0$ m, and $y_{G,n} = 0.40$ m. | 45 |
| 5.9 | Maximum velocity for the crouching groom dependent on the steering angle for combinations of $x_{G,1} = -0.30$ m, and $x_{G,n} = -0.50$ m with $y_{G,1} = 0$ m, and $y_{G,n} = 0.40$ m. | 45 |
| 5.10 | Maximum velocity dependent on the relative position of the sitting groom. | 47 |
| 5.11 | Maximum velocity for the groom dependent on the radius of curvature of the turn for $x_{G,rel} = -0.22$ m with $y_{G,in} = 0.60$ m, and $y_{G,out} = -0.60$ m. | 49 |
| 5.12 | Maximum velocity for the groom dependent steering angle for $x_{G,rel} = -0.22$ m with $y_{G,in} = 0.60$ m, and $y_{G,out} = -0.60$ m. | 49 |
| 5.13 | Maximum velocity of point mass model and model with inertia-tensor. | 50 |
| 5.14 | Maximum velocity dependent on the steering angle for combinations of $x_{G,1} = -0.15$ m, and $x_{G,n} = -0.50$ m with $y_{G,1} = 0$ m, and $y_{G,n} = 0.40$ m. | 51 |
| 5.15 | Maximum velocity dependent on the relative position of the groom. | 52 |
| 5.16 | Lines of constant velocity dependent on the relative position of the groom. | 52 |
| 5.17 | Maximum velocity dependent on the radius of curvature of the turn. | 53 |
| 5.18 | Maximum velocity dependent on the steering angle. | 54 |
| 5.19 | Maximum velocity dependent on the relative position of standing p50-groom. | 55 |
| 5.20 | Lines of constant velocity dependent on the relative position of the p50-groom. | 55 |
| 5.21 | Lines of constant velocity dependent on the relative position of the p50-groom. | 56 |
| 5.22 | Maximum velocity dependent on the steering angle for combinations of $x_{G,1} = -0.15$ m, and $x_{G,n} = -0.50$ m with $y_{G,1} = 0$ m, and $y_{G,n} = 0.40$ m. | 57 |

List of Tables

| | | |
|------|--|----|
| 2.1 | Moment and product of inertia of the area model. | 7 |
| 2.2 | Moment and product of inertia of the rod model. | 7 |
| 2.3 | Additional carriage data. | 8 |
| 2.4 | Moment and product of inertia of the rod model of a dressage carriage. | 9 |
| 2.5 | Influence of parallel axis theorem. | 10 |
| 2.6 | Measured data including estimated errors. | 11 |
| 2.7 | Calculated moment of inertia of wheels. | 12 |
| 3.1 | Moment and product of inertia as well as the centre of gravity of the driver. | 17 |
| 3.2 | Ranges for the values of moment and product of inertia as well as position of the centre of gravity of the driver. | 17 |
| 3.3 | Moment and product of inertia as well as the centre of gravity of the standing groom. | 19 |
| 3.4 | Ranges for the values of moment and product of inertia as well as position of the centre of gravity of the standing groom. | 19 |
| 3.5 | Moment and product of inertia as well as the centre of gravity of the groom sitting straight. | 21 |
| 3.6 | Ranges for the values of moment and product of inertia as well as position of the centre of gravity of the straight sitting groom. | 21 |
| 3.7 | Moment and product of inertia as well as the centre of gravity of the groom leaning. | 23 |
| 3.8 | Ranges for the values of moment and product of inertia as well as position of the centre of gravity of the leaning groom. | 23 |
| 3.9 | Moment and product of inertia as well as the centre of gravity of the sitting groom with stretched leg. | 24 |
| 3.10 | Ranges for the values of moment and product of inertia as well as position of the centre of gravity of the sitting groom with stretched leg. | 24 |
| 3.11 | Moment and product of inertia as well as the centre of gravity of the leaning groom with stretched leg. | 26 |
| 3.12 | Ranges for the values of moment and product of inertia as well as position of the centre of gravity of the leaning groom with stretched leg. | 26 |

| | | |
|------|--|----|
| 3.13 | Moment and product of inertia as well as the centre of gravity of the crouching groom. | 28 |
| 3.14 | Ranges for the values of moment and product of inertia as well as position of the centre of gravity of the crouching groom. | 28 |
| 3.15 | Moment and product of inertia as well as the centre of gravity of the groom on dressage carriage. | 30 |
| 3.16 | Ranges for the values of moment and product of inertia as well as position of the centre of gravity of the groom on dressage carriage. . . | 30 |
| 5.1 | Location range of the reference point of the standing groom. | 38 |
| 5.2 | Maximum velocity (in m/s) for different driver and standing groom combinations at the four corner-positions and in the plane of symmetry and $r_C = -2$ m. | 38 |
| 5.3 | Location range of the reference point of the sitting groom. | 41 |
| 5.4 | Maximum velocity (in m/s) for different driver and sitting groom combinations at the four corner-positions at $r_C = -2$ m. | 41 |
| 5.5 | Location range of the reference point of the crouching groom. | 44 |
| 5.6 | Maximum velocity (in m/s) for different driver and crouching groom combinations at the four corner-positions at $r_C = -2$ m. | 44 |
| 5.7 | Location range of the reference point of the groom on dressage carriage. | 48 |
| 5.8 | Maximum velocity (in m/s) for different driver and groom combinations on a dressage carriage at $r_C = -2$ m. | 48 |
| 5.9 | Maximum velocity for -2 m curves with or without inertia-tensor. . . | 51 |
| B.1 | Necessary input data for <code>marathon_carriage_data.m</code> | 66 |
| B.2 | Necessary input data for <code>dressage_carriage_data.m</code> | 67 |
| C.1 | Input data for modelling the driver. | 68 |
| C.2 | Input data for modelling the standing groom. | 69 |
| C.3 | Input data for modelling the straight sitting groom. | 69 |
| C.4 | Input data for modelling the leaning groom. | 69 |
| C.5 | Input data for modelling the straight sitting groom with stretched leg. | 69 |
| C.6 | Input data for modelling the leaning groom with stretched leg. | 70 |
| C.7 | Input data for modelling the crouching groom. | 70 |
| C.8 | Input data for modelling the sitting groom on dressage carriage. | 70 |

Appendix A

Listing of the main MATLAB functions

| Main script files | Description |
|--------------------------|---|
| marathon_carriage_data.m | Generates and saves model of marathon carriage |
| dressage_carriage_data.m | Generates and saves model of dressage carriage |
| GenerateHuman.m | Generates and saves model of human |
| LoadHuman.m | Loads model of human and allows parameter changes |
| SimulateCarriage.m | Runs dynamic simulation and saves results |

| Main function files | Description |
|---------------------|---|
| IS_wheel.m | Generates inertia of wheel |
| IS_turntable.m | Generates and plots model of front axle |
| carriage_draw.m | Generates plot of rod model of carriage |
| calc_joint_front.m | Calculates forces of wheels for multiple groom positions for model with ball joint in front |
| calc_vel.m | Calculates maximal inertia for multiple groom positions for model with ball joint in front |
| plot_velocity.m | Generates surface and contour plot of calculated velocity |

Appendix B

Input data for carriage modelling

B.1 Marathon carriage

Table B.1: Necessary input data for `marathon_carriage_data.m`.

| geometry of marathon carriage (in m) | |
|--------------------------------------|--|
| <code>l_C = 1.50;</code> | length of entire carriage |
| <code>l_W = 0.94;</code> | wheelbase of carriage |
| <code>w_F = 1.25;</code> | track width front |
| <code>w_R = 1.25;</code> | track width back |
| <code>angle_tip = 44;</code> | angle of tipping (in °) |
| <code>d_TT = 0.3;</code> | diameter of turntable |
| <code>x_sf = 0.42;</code> | location of centre of front seat in x |
| <code>y_sf = 0;</code> | location of centre of front seat in y |
| <code>h_sf = 1.25;</code> | height of front seat |
| <code>a_sf = 0.525;</code> | length of front seat area (seat considered as square) |
| <code>x_sb = -0.22;</code> | location of centre of sitting in back in x |
| <code>y_sb = -0.54;</code> | location of centre of sitting in back in y |
| <code>h_sb = 0.88;</code> | height of rear seat |
| <code>a_sb = 0.51;</code> | length of rear seat (rear seat considered as triangle) |
| <code>b_sb = 0.35;</code> | width of rear seat (rear seat considered as triangle) |
| <code>h_fm = 0.81;</code> | height of main floor |
| <code>a_fm = 1.03;</code> | length of main floor |
| <code>b_fm = 1.25;</code> | width of main floor |
| <code>x_fm = 0.07;</code> | distance between back axle and main floor in x |
| <code>angle_ff = 45;</code> | angle of front floor (in °) |
| <code>a_ff = 0.35;</code> | length of front floor |
| <code>b_ff = 0.85;</code> | width of front floor |
| <code>h_fb = 0.35;</code> | height of back floor |
| <code>a_fb = 0.385;</code> | length of back floor |
| <code>b1_fb = 0.57;</code> | small width of back floor |
| <code>b2_fb = 1.0;</code> | large width of back floor |
| <code>x_fb = -0.5;</code> | distance between rear axle and rear end of floor |
| <code>h_sfr = h_fm+0.14;</code> | height of rod of front seat |
| <code>d_WF = 0.748;</code> | diameter of front wheels |
| <code>d_WR = d_WF;</code> | diameter of rear wheels |
| <code>w_WF = 0.04;</code> | width of wheels front |
| <code>w_WR = 0.04;</code> | width of rear wheels |
| masses of carriage (in kg) | |
| <code>m_F = 102;</code> | mass in front (including wheels) |
| <code>m_B = 102;</code> | mass in rear (including wheels) |
| <code>m_all = m_F+m_B;</code> | mass of carriage (including wheels) |
| <code>m_WF = 11.5;</code> | mass of front wheels |
| <code>m_WR = m_WF;</code> | mass of back wheels |
| <code>m_sf = 0;</code> | mass of front seat |
| <code>m_TT = 2*29-2*m_WF;</code> | mass of turntable |

B.2 Dressage carriage

Table B.2: Necessary input data for `dressage_carriage_data.m`.

| geometry of dressage carriage (in m) | |
|--------------------------------------|--|
| <code>l_W = 1.145;</code> | wheelbase of carriage |
| <code>w_F = 1.4;</code> | track width front |
| <code>w_R = 1.4;</code> | track width rear |
| <code>angle_tip = 49;</code> | angle of tipping (in °) |
| <code>x_sf = 0.69;</code> | location of centre of front seat in x |
| <code>y_sf = 0;</code> | location of centre of front seat in y |
| <code>h_sf = 1.40;</code> | height of front seat |
| <code>a_sf = 0.39;</code> | length of front seat area |
| <code>b_sf = 0.48;</code> | width of front seat |
| <code>x_sb = -0.22;</code> | location of centre of sitting in back in x |
| <code>y_sb = -0.0;</code> | location of centre of sitting in back in y |
| <code>h_sb = 1.34;</code> | height of rear seat |
| <code>a_sb = 0.39;</code> | length of rear seat |
| <code>b_sb = 0.48;</code> | width of rear seat |
| <code>h_fm = 0.825;</code> | height of main floor |
| <code>b_fm = 0.836;</code> | width of main floor |
| <code>a_fb = 0.65;</code> | length of rear floor |
| <code>x_fm = -0.32;</code> | distance between rear axle and main floor in x |
| <code>a1_fs = 0.4;</code> | upper length of seat floor |
| <code>a2_fs = 0.6;</code> | lower length of seat floor |
| <code>h_fs = 1.18;</code> | height of seat floor |
| <code>a_ff = 0.635;</code> | length of front floor |
| <code>c_ff = 0.48;</code> | height of front wall |
| <code>d_TT = 0.4;</code> | diameter of turntable |
| <code>d_WF = 0.795;</code> | diameter of front wheels |
| <code>d_WR = 0.994;</code> | diameter of rear wheels |
| <code>w_WF = 0.045;</code> | width of front wheels |
| <code>w_WR = 0.045;</code> | width of rear wheels |
| masses of carriage (in kg) | |
| <code>m_F = 158;</code> | mass in front (including wheels) |
| <code>m_R = 136;</code> | mass in rear (including wheels) |
| <code>m_all = m_F+m_R;</code> | mass of carriage (including wheels) |
| <code>m_WF = 13.5;</code> | mass of front wheels |
| <code>m_WR = 19.5;</code> | mass of rear wheels |
| <code>m_TT = 2*44-2*m_WF;</code> | mass of turntable |

Appendix C

Input data for human modelling

Here the necessary input data for generating a human model using the MATLAB skript `GenerateHuman.m` is given. In order to generate a certain posture, the joint angles for each segment must be defined.

Here, this was done in `jntang_deg` in deg, these values then need to be converted into rad. The matrix `jntang_deg` contains all rotational angles of a segment relative to the segment it is attached to, starting from segment3, the lower torso. The rows of `jntang_deg` contain the rotation around the x , y and z -axis. The columns represent the segment number, as defined by Hanavan in [6].

After defining the posture, the position of the dummy has to be defined via the lower torso (segment 3). Therefore, the angle and the location of the lower torso are defined separately in `ang3_deg` and `cm3`. The angles of `ang3_deg` are given in deg and need to be converted to rad. The vector of displacement `cm3` is given either in m or a corresponding MATLAB variable. The coordinates of segment 3 are defined relative to the centre of mass of the lower torso.

Table C.1: Input data for modelling the driver.

| jntang_deg = | | | | | | | | | | | | | |
|--------------|-----|---|---|-----|----|--------|-------|-----|----|-----|-----|----|----|
| 0 | 0 | 0 | 0 | -30 | 30 | 0 | 0 | 0 | 0 | 0 | 0 | 90 | 90 |
| 0 | -10 | 0 | 0 | 70 | 70 | 50 | 50 | 85 | 85 | -30 | -30 | 0 | 0 |
| 0 | 0 | 0 | 0 | 0 | 0 | -11.25 | 11.25 | -15 | 15 | 0 | 0 | 90 | 90 |

| ang3_deg = | | | cm3 = |
|------------|-----|-----|---------|
| p25 | p50 | p75 | ... |
| 0 | 0 | 0 | 0 |
| 12 | 11 | 10 | 0 |
| 180 | 180 | 180 | s1(3)/2 |

Table C.2: Input data for modelling the standing groom.

| jntang_deg = | | | | | | | | | | | | | |
|--------------|-----|---|---|-----|----|-----|----|-----|----|-----|-----|-----|-----|
| 0 | 0 | 0 | 0 | -30 | 30 | 0 | 0 | 0 | 0 | 0 | 0 | 90 | 90 |
| 0 | -10 | 0 | 0 | 80 | 80 | 30 | 30 | 10 | 10 | -20 | -20 | 0 | 0 |
| 0 | 0 | 0 | 0 | 0 | 0 | -25 | 25 | -10 | 10 | 0 | 0 | 100 | 100 |

| ang3_deg = | cm3 = | | |
|------------|--------|--------|--------|
| ... | p25 | p50 | p75 |
| 0 | 0 | 0 | 0 |
| 0 | 0 | 0 | 0 |
| 180 | 0.9530 | 0.9764 | 1.0010 |

Table C.3: Input data for modelling the straight sitting groom.

| jntang_deg = | | | | | | | | | | | | | |
|--------------|-----|---|---|----|-----|-----|-----|----|----|-----|-----|----|----|
| 0 | 0 | 0 | 0 | 10 | -10 | 0 | 0 | 0 | 0 | 0 | 0 | 90 | 90 |
| 0 | -10 | 0 | 0 | 90 | 140 | -20 | -15 | 60 | 60 | -70 | -70 | 0 | 0 |
| 0 | 0 | 0 | 0 | 0 | 0 | -15 | 15 | 0 | 0 | 0 | 0 | 90 | 90 |

| ang3_deg = | cm3 = |
|------------|---------|
| -110 | 0 |
| -10 | 0 |
| 180 | sl(3)/2 |

Table C.4: Input data for modelling the leaning groom.

| jntang_deg = | | | | | | | | | | | | | |
|--------------|-----|---|---|----|-----|-----|-----|----|----|-----|-----|----|----|
| 0 | 0 | 0 | 0 | 10 | -10 | 0 | 0 | 0 | 0 | 0 | 0 | 90 | 90 |
| 0 | -10 | 0 | 0 | 65 | 120 | -5 | -15 | 40 | 40 | -70 | -70 | 0 | 0 |
| 0 | 0 | 0 | 0 | 5 | -5 | -10 | 10 | 0 | 0 | 0 | 0 | 90 | 90 |

| ang3_deg = | cm3 = | | |
|------------|--------|--------|--------|
| ... | p25 | p50 | p75 |
| -110 | 0.0139 | 0.0136 | 0.0133 |
| -30 | 0.0381 | 0.0374 | 0.0366 |
| 180 | 0.1757 | 0.1791 | 0.1916 |

Table C.5: Input data for modelling the straight sitting groom with stretched leg.

| jntang_deg = | | | | | | | | | | | | | |
|--------------|-----|---|---|----|-----|-----|-----|----|----|-----|-----|----|----|
| 0 | 0 | 0 | 0 | 10 | -10 | 0 | 0 | 0 | 0 | 0 | 0 | 90 | 90 |
| 0 | -10 | 0 | 0 | 90 | 140 | -20 | -15 | 60 | 60 | -70 | -20 | 0 | 0 |
| 0 | 0 | 0 | 0 | 0 | 0 | -15 | 15 | 0 | 0 | 0 | 0 | 90 | 90 |

| ang3_deg = | cm3 = |
|------------|---------|
| -110 | 0 |
| -10 | 0 |
| 180 | sl(3)/2 |

Table C.6: Input data for modelling the leaning groom with stretched leg.

| jntang_deg = | | | | | | | | | | | | | |
|--------------|-----|---|---|----|-----|-----|-----|----|----|-----|-----|----|----|
| 0 | 0 | 0 | 0 | 10 | -10 | 0 | 0 | 0 | 0 | 0 | 0 | 90 | 90 |
| 0 | -10 | 0 | 0 | 65 | 120 | -5 | -15 | 40 | 40 | -70 | -20 | 0 | 0 |
| 0 | 0 | 0 | 0 | 5 | -5 | -10 | 10 | 0 | 0 | 0 | 0 | 90 | 90 |

| ang3_deg = | | cm3 = | | |
|------------|--|--------|--------|--------|
| ... | | p25 | p50 | p75 |
| -110 | | 0.0139 | 0.0136 | 0.0133 |
| -30 | | 0.0381 | 0.0374 | 0.0366 |
| 180 | | 0.1757 | 0.1791 | 0.1916 |

Table C.7: Input data for modelling the crouching groom.

| jntang_deg = | | | | | | | | | | | | | |
|--------------|-----|---|---|----|-----|-----|----|-----|-----|------|------|-----|-----|
| 0 | -10 | 0 | 0 | 0 | 0 | 0 | 30 | 0 | 0 | 0 | 0 | 90 | 90 |
| 0 | -10 | 0 | 0 | 10 | 150 | 130 | 20 | 115 | 115 | -110 | -110 | 0 | 0 |
| 0 | 0 | 0 | 0 | 10 | -5 | -20 | 20 | 0 | 0 | 0 | 0 | 100 | 100 |

| ang3_deg = | | cm3 = | | |
|------------|--|---------|---------|---------|
| ... | | p25 | p50 | p75 |
| 0 | | -0.3436 | -0.3546 | -0.3656 |
| 15 | | 0 | 0 | 0 |
| 180 | | 0.4434 | 0.4525 | 0.4629 |

Table C.8: Input data for modelling the sitting groom on dressage carriage.

| jntang_deg = | | | | | | | | | | | | | |
|--------------|-----|---|---|-----|----|--------|-------|-----|----|-----|-----|----|----|
| 0 | 0 | 0 | 0 | -10 | 10 | 0 | 0 | 0 | 0 | 0 | 0 | 90 | 90 |
| 0 | -10 | 0 | 0 | 90 | 90 | -30 | -30 | 85 | 85 | -60 | -60 | 0 | 0 |
| 0 | 0 | 0 | 0 | 0 | 0 | -11.25 | 11.25 | -15 | 15 | 0 | 0 | 90 | 90 |

| ang3_deg = | | | cm3 = | |
|------------|-----|-----|---------|--|
| p25 | p50 | p75 | ... | |
| 0 | 0 | 0 | 0 | |
| 12 | 11 | 10 | 0 | |
| 180 | 180 | 180 | s1(3)/2 | |

Bibliography

- [1] W. N. Bao. Analysis and simulation on vehicle rollover dynamic driving on curving path. In *Advanced Materials Research*, volume 834, pages 1347–1350. Trans Tech Publ, 2014.
- [2] R. Chandler, C. E. Clauser, J. T. McConville, H. Reynolds, and J. W. Young. *Investigation of inertial properties of the human body*. Aerospace Medical Research Laboratories, Wright-Patterson Air Force Base, Ohio, 1975.
- [3] C. E. Clauser, J. T. McConville, and J. W. Young. *Weight, volume, and center of mass of segments of the human body*. Aerospace Medical Research Laboratories, Wright-Patterson Air Force Base, Ohio, 1969.
- [4] G.-M. Dong, N. Zhang, and H.-P. Du. Investigation into untripped rollover of light vehicles in the modified fishhook and the sine manoeuvres, part II: effects of vehicle inertia property, suspension and tyre characteristics. *Vehicle System Dynamics*, 49(6):949–968, 2011.
- [5] J. Fleck and F. Butler. *Development of an improved computer model of the human body and extremity dynamics*. Aerospace Medical Research Laboratories, Wright-Patterson Air Force Base, Ohio, 1975.
- [6] E. Hanavan. *A mathematical model of the human body*. Aerospace Medical Research Laboratories, Wright-Patterson Air Force Base, Ohio, 1964.
- [7] H. Hatze. A mathematical model for the computational determination of parameter values of anthropomorphic segments. *Journal of Biomechanics*, 13(10):833–843, 1980.
- [8] G. Hughes. Trifilar pendulum and its application to experimental determination of moments of inertia. *ASME Papers*, 57, 1957.
- [9] J. C. Huston, B. J. Graves, and D. B. Johnson. Three wheeled vehicle dynamics. Technical report, SAE Technical Paper 820139, 1982.

-
- [10] F. Klinger, J. Nusime, J. Edelmann, and M. Plöchl. Wobble of a racing bicycle with a rider hands on and hands off the handlebar. *Vehicle System Dynamics*, 52(sup1):51–68, 2014.
 - [11] H. Parkus. *Mechanik der festen Körper*. Springer-Verlag, 2013.
 - [12] W. R. Santschi, J. Dubois, and C. Omoto. *Moments of inertia and centers of gravity of the living human body*. Aerospace Medical Research Laboratories, Wright-Patterson Air Force Base, Ohio, 1963.
 - [13] R. A. Serway. *Physics for Scientists and Engineers*. Saunders College Publishing, 1986.
 - [14] P. G. Van Valkenburgh, R. H. Klein, and J. Kanianthra. Three-wheel passenger vehicle stability and handling. Technical report, SAE Technical Paper 820140, 1982.
 - [15] C. E. Whitsett. *Some dynamic response characteristics of weightless man*. Aerospace Medical Research Laboratories, Wright-Patterson Air Force Base, Ohio, 1963.
 - [16] M. Yeadon. The simulation of aerial movement—II. A mathematical inertia model of the human body. *Journal of Biomechanics*, 23(1):67 – 74, 1990.
 - [17] N. Zhang, G.-M. Dong, and H.-P. Du. Investigation into untripped rollover of light vehicles in the modified fishhook and the sine maneuvers. part I: Vehicle modelling, roll and yaw instability. *Vehicle System Dynamics*, 46(4):271–293, 2008.